UC Santa Cruz
UC Santa Cruz Electronic Theses and Dissertations

Title
Atomic cooling via AC Stark shift

Permalink
https://escholarship.org/uc/item/41t528jv

Author
Black, Jennifer Anne

Publication Date
2014

Peer reviewed|Thesis/dissertation

UNIVERSITY OF CALIFORNIA

SANTA CRUZ

ATOMIC COOLING VIA AC STARK SHIFT

A thesis submitted in partial satisfaction
of the requirements for the degree of

MASTER OF SCIENCE

in

PHYSICS

by

Jennifer Black

September 2014

The Thesis of Jennifer Black
is approved by:

_____
Professor Sue Carter, chair

_____
Professor Holger Schmidt

_____
Professor Gey-Hong Gweon

_____

Tyrus Miller
Vice Provost and Dean of Graduate Studies

Table of Contents

List of Figures

List of Tables

Abstract

ATOMIC COOLING VIA AC STARK SHIFT

by

Jennifer Black

Described in this thesis is a new all optical approach to atomic cooling [1]. This approach is ideally suited for waveguide based atom photonic platforms and here we present two design methods to achieving cooling of sodium (Na) atoms using anti-resonant reflecting optical waveguides (ARROWs). The proposed devices could cool Na atoms to 1.47 K corresponding to a mean speed of 40 m/s which is comparable to Zeeman based cooling techniques. The methods presented here however are amenable to free space setups as well as other waveguide devices and are applicable to other atomic species.

Acknowledgements

I would like to thank my advisor, Dr. Holger Schmidt for his guidance. He has been a wealth of knowledge and continually patient with me. Graduate school is hard! Thanks to everyone who makes it bearable. Such people include my wonderful lab mates who I am so grateful to have around 40 plus hours a week, my family who though they are an entire nation away are always loving and supportive, my friends who have enriched my experience in Santa Cruz and of course my loving husband, Jonathan Bruce.

Chapter 1

Introduction

Decades ago, radiation pressure was found to create observable forces on particles and near resonant atoms [2], [3]. However, the application to atoms did not receive much interest until the advent of tunable lasers with higher powers and in 1975 Hänsch and Schawlow [4] proposed that such light sources could be used to cool atoms. Eventually, an independent research field based on optical slowing and trapping of atoms for applications in precision metrology and fundamental studies of quantum matter developed [5].

One of the earliest techniques, single beam cooling, relies on the repeated resonant absorption of photons from a directed beam that opposes the atom's motion. The momentum change afforded by isotropic re-radiation via spontaneous emission slows and thus cools the atom down. In practice, this cooling beam needs to be red shifted from the atomic transition frequency in order to account for the Doppler shift of $\frac{2\pi v_o}{\lambda}$ where v_o is the atom's initial speed and λ the laser wavelength. The problem is that as an atom slows, the Doppler shifted frequency of the beam falls from resonance, and the atom will eventually be unable to absorb any more photons.

There are two common remedies to compensate for this dynamic Doppler shift ΔE_{D}. One solution is to chirp the laser to progressively higher frequencies in

order to keep it on resonance [6]. The second method uses a spatially varying magnetic field along z, the direction of deceleration, to move the atom's energy levels via the Zeeman Effect [7]. Here, we introduce a new all-optical method for Doppler compensation in atomic cooling based on a spatially varying AC Stark shift. Our goal is to attain final speeds comparable to Zeeman slowers which could be used to load a magneto-optical trap without the additional required apparatus to create a suitable inhomogeneous magnetic field [8]. The AC Stark shift, ΔE_{AC}, is an intensity based shift that lowers the electronic ground state for a red-tuned beam [9]. Therefore, an AC Stark beam can increase the atomic resonance frequency to compensate for the apparent lowering due to the Doppler shift, and the atoms can continually cool if $\Delta E_{\text{AC}}(z) + \Delta E_{\text{D}}(z) = 0$ is satisfied.

This thesis is structured as follows: Chapter 2 presents theoretical background on atomic physics and light-matter interactions necessary to understanding our proposed devices. Chapter 3 discusses the principles of anti-resonant reflecting optical waveguides (ARROWs) and how loss calculations in such waveguides are performed. In Chapter 4, the principle for an AC Stark slower is described and two waveguide designs using ARROWs are presented using the theoretical framework built in previous sections. Finally, Chapter 5 presents future outlooks of this technology and concludes this thesis.

Chapter 2

Light-Matter Interactions

The following chapter introduces several theoretical concepts necessary in understanding AC Stark cooling. Here we also describe two common methods to atomic cooling that are currently used in order to highlight the motivation for our proposed technique.

2.1 Radiation Pressure

Radiation pressure in atoms is a result of scattering photons (cycles of absorption and emission). Consider an atom that is counter-propagating with a laser of wavevector $k = \frac{2\pi}{\lambda} = |\vec{k}|$ as seen in Fig. 2.1. If the laser's wavelength is near atomic resonance then it can be absorbed by the atom, and via conservation of momentum the atom's new momentum is given by $mv - \hbar k$. Consequently, the atom decelerates and is then able to spontaneously emit the photon which again results in a momentum change of magnitude $\hbar k$ as the atom falls back to the ground state. The net change in momentum from spontaneous emission over many scattering cycles is zero, thus allowing for the atom to decelerate. However, spontaneous emission may contribute to increasing velocities transverse to the direction of deceleration (or

transverse heating), which if not ameliorated, will distort the atomic beam's

collimation. Transverse heating will be discussed further in section 2.7.

Fig. 2.1: An atom with momentum $m\vec{v}$ can absorb a counter-propagating photon of momentum $\hbar\vec{k}$ if its frequency appears on resonance.

The atom's change in velocity after absorption of one photon is called the

recoil velocity, $v_r = \frac{\hbar k}{m}$. Considering Sodium (Na) atoms absorbing light near its D_2

hyperfine resonance, $\lambda = 589.16$ nm with mass, $m = 0.3818 \times 10^{-25}$ kg, we find

$v_r = 2.9461$ cm/s. Though this is a small change in speed, Na is able to absorb many

photons in a short amount of time. The rate at which an atom can go through this

scattering cycle is aptly named the scattering rate and is given by [10]

$$R = \left(\frac{\Gamma}{2}\right) \frac{\left(I/I_{sat}\right)}{1 + 4\left(\Delta/\Gamma\right)^2 + \left(I/I_{sat}\right)} \quad (2.1)$$

Where Γ is the lifetime of an atomic transition, $\Delta = \omega_L - \omega_o$ is the detuning of the

laser, ω_L, from resonance, ω_o, I is the intensity of the light and I_{sat} the saturation

intensity given by

$$I_{sat} = \frac{c\varepsilon_o \Gamma^2 \hbar^2}{4|\hat{\varepsilon} \cdot \vec{\mu}|^2} \quad (2.2)$$

Where c is the speed of light, $\hbar$ is the reduced Plank constant, ε_o the permittivity of

free space, $\hat{\varepsilon}$ is the polarization unit vector and $\vec{\mu}$ is the atomic dipole moment for the

relevant transition. When a high intensity beam is present ($I \gg I_{sat}$), the scattering

rate (2.1) goes to $\frac{\Gamma}{2}$. The magnitude of deceleration of an atom due to this scattering

process is $a = \frac{|\Delta\vec{p}|}{m\Delta t} = \frac{hR}{m\lambda}$ which goes to $\frac{h\Gamma}{2m\lambda}$ in the saturated limit. For the Na D_2

hyperfine transitions, the magnitude of saturation limited deceleration is 9.0643 x

$10^5 \frac{m}{s^2}$.

The mean speed of atoms at a given temperature is expressed as

$$v = \sqrt{\frac{8k_B T}{\pi M}} \quad (2.3)$$

Where M is the mass, k_B is the Boltzmann constant and T is the temperature in

Kelvin. So, Na atoms at room temperature (T ~ 300 K) have a mean velocity of 525.6

m/s. In order to slow them to a final velocity of 10 m/s, the Na atoms must absorb

$N = \frac{(525.6-10)\ m/s}{v_r} \approx 1.75$ x 10^4 photons which in the saturated limit will take 0.54

ms. Using the Galilean equations of motion, we can also determine the necessary

length, L, needed to slow atoms from room temperature speeds to 10 m/s: $L =$

$\frac{10^2 - 525.6^2}{-2*(9.0643 \text{ x } 10^5)} = 15.23$ cm. Thus, the lengths necessary for the slowing of Na atoms

to speeds of tens of meters per second are achievable on the chip scale. The relevant

values for Na mentioned above are summarized in appendix A.

2.2 Doppler Shift

To an atom, the apparent detuning of a laser from an atomic resonance is

dependent on the atom's velocity relative to the direction of propagation of the laser.

This difference in frequency from the lab's perspective is known as the Doppler shift. The amount of detuning seen by the atom is given by

$$\Delta = \delta_L - \vec{k} \cdot \vec{v} \quad (2.4)$$

Where δ_L is the detuning of the laser in the lab reference frame and the Doppler shift is given by $-\vec{k} \cdot \vec{v}$. The scenario described above for atomic cooling consisted of an atom counter-propagating with a laser and as the atom absorbs the photons, it will slow. However, in order for the atom to be able to absorb the atoms, the laser must appear near resonance. If a laser which in the lab frame is locked to resonance for a Na atom's transition, it will appear blue shifted to an atom moving in the opposite direction of the beam because $\vec{k} \cdot \vec{v} < 0$. So, as seen in Fig. 2.2, one must set the laser frequency, ω_L to be red-detuned by the Doppler shift ($-\vec{k} \cdot \vec{v}$) in order to make the laser appear on resonance.
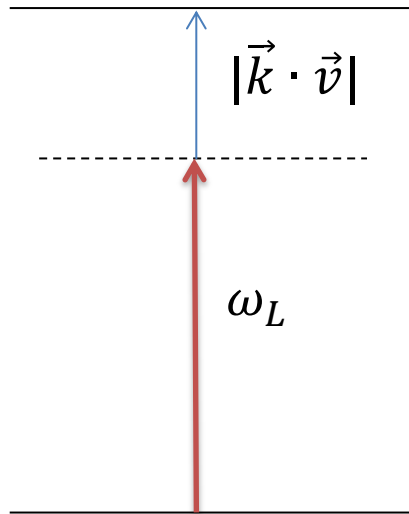
Fig. 2.2: A counter-propagating laser can be absorbed if it is red-detuned by the Doppler shift, thus making it appear on resonance.

Since a Na atom near room temperature has a speed of 500 m/s, one finds a non-negligible Doppler shift (~ $2\pi \cdot 0.9$ GHz) and thus the Doppler cooling beam must be red shifted in the lab frame ($\delta_L < 0$) in order to compensate for the Doppler shift. Then, as its speed is reduced, the required Doppler shift will change continuously as the atom slows down and the atom will eventually be unable to absorb any more photons as the atom now sees the laser closer to its red shifted frequency chosen in the lab reference frame. There are two common remedies to this problem: Zeeman assisted cooling and chirping of the cooling beam. The proposed AC Stark slowing presented here is analogous to Zeeman slowing where instead of using a magnetic field to provide an appropriate shift in the ground state, a detuned electric field can be used whose intensity is proportional to the ground state energy shift.

2.3 Zeeman Slowing
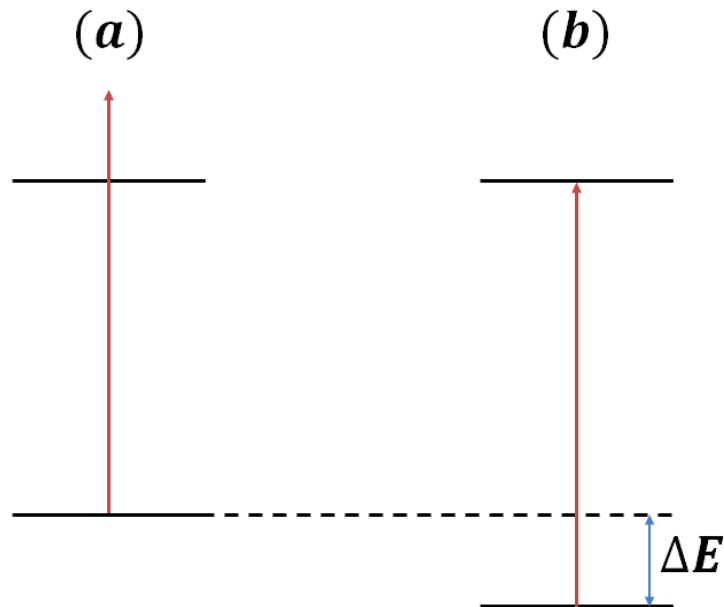
Fig. 2.3: (a) No magnetic field present. Apparent cooling frequency blue shifted due to the counter-propagating velocity induced Doppler shift. (b) Magnetic field present. Zeeman shift of the ground state allows the blue shifted cooling beam to appear on resonance.

Zeeman assisted cooling uses a fixed frequency Doppler cooling beam and a spatially varying magnetic field [11]. The Doppler cooling beam can either be chosen at an atomic transition's resonance or detuned. The purpose of the magnetic field is to provide an appropriate Zeeman shift of the ground state in order to make the Doppler cooling beam continually appear on resonance as the atom slows. If the Doppler cooling beam is on resonance in the lab frame, then a counter-propagating atom will see the beam blue shifted as described in the previous section. Thus, the atom will see the beam blue shifted as seen in Fig. 2.3.a. If an appropriate Zeeman shift is present then the ground state can be lowered and the seemingly blue shifted cooling beam can be absorbed as seen in Fig. 2.3.b.

As the atom cools, the Doppler shift changes and thus the Zeeman shift must also vary along the direction of deceleration, z. In order to achieve such an inhomogeneous magnetic field, an intricate solenoid is constructed. The strength of the magnetic field at a given position along z is determined by the number of coils (N) a wire makes in the radial direction from z. In order to determine what the magnetic field profile must look like, we must first determine the Doppler shift as a function of z. In the saturated limit, the deceleration due to absorption of the cooling beam goes to $|\vec{a}| = \frac{h\Gamma}{2m\lambda}$ as described in section 2.1. Assuming constant deceleration (continued absorption) along z, one can write the atom's velocity along z as $v(z) = \sqrt{v_0^2 + 2az}$ where v_0 is determined by the initial temperature of the atoms (equation 2.3). Then the Doppler shift can be written:

$$\Delta E_D(z) = \frac{h}{\lambda}v(z) = \frac{h}{\lambda}\sqrt{v_0^2 + 2az} \quad (2.5)$$

The desired Zeeman shift (ΔE_Z) must satisfy the following condition in order to ensure constant deceleration:

$$\Delta E_Z(z) + \Delta E_D(z) = 0 \quad (2.6)$$

The linear Zeeman shift can be found using the interaction Hamiltonian:

$$H_{int} = \vec{\mu} \cdot \vec{B} = \frac{\mu_B}{\hbar}\left(g_L\vec{L} + g_S\vec{S} + g_I\vec{I}\right) \cdot \vec{B} \quad (2.7)$$

Where μ_B is the Bohr magneton, $\hbar$ is the reduced Planck constant, g_L, g_S and g_I are the electron orbital, spin and nuclear Landé g-factors respectively. Taking the magnetic field to be along the z-direction we can write

$$H_{int} = \frac{\mu_B}{\hbar}(g_L L_z + g_S S_z + g_I I_z)B = \frac{\mu_B}{\hbar}(g_F F_z)B \quad (2.8)$$

Where $B \equiv \left|\overrightarrow{B(z)}\right|$ and $F = J + I = L + S + I$ (see section 2.6). Using first order

perturbation theory, we can find the Zeeman light shift via [10], [12]:

$$\Delta E_Z = \langle F, m_F | H_{int} | F, m_F \rangle = \frac{\mu_B}{\hbar} g_F B \langle F, m_F | F_z | F, m_F \rangle = \mu_B g_F m_F B \quad (2.9)$$

Using this along with equation 2.5 and 2.6, the magnetic field along z must take the

following form:

$$B(z) = \frac{-h}{\lambda \mu_B g_F m_F} \sqrt{v_0{}^2 + 2az} \quad (2.10)$$

Now that the magnetic field profile is specified, one must construct such a

field. Using the Biot-Savart Law one can determine the number of loops the wire

must make along the slowing axis within a step along z thus defining the shape of the

taper the solenoid must make along z. A rough schematic of such a Zeeman slower is

shown in Fig. 2.4 after [5].
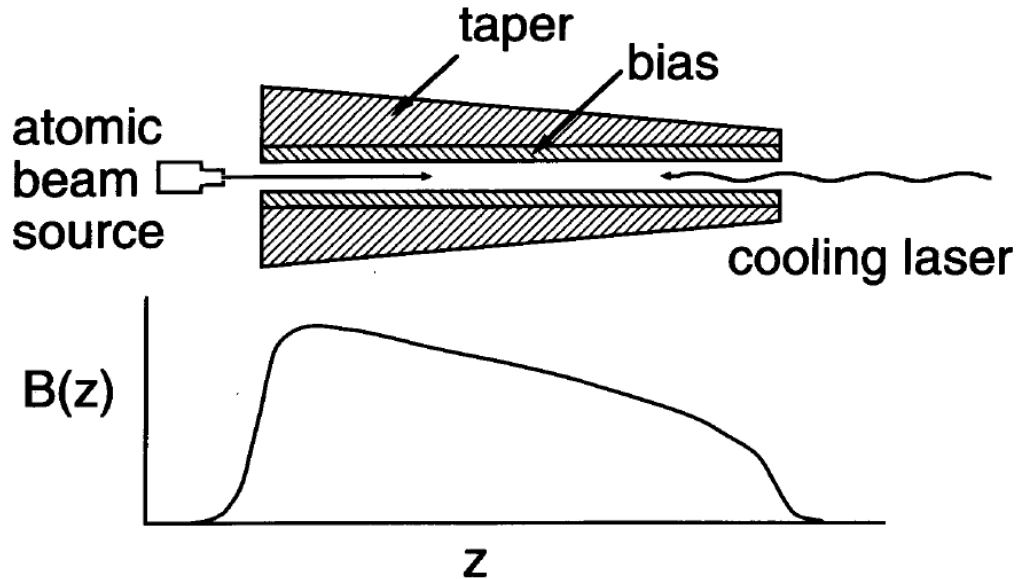
Fig. 2.4: A schematic of a typical Zeeman slower along with the corresponding
inhomogeneous magnetic field along the direction of cooling, z. From ref [5].

2.4 Chirped Slowing

Another method for Doppler cooling involves the chirping of the cooling beam. This means that the cooling beam's frequency is shifted in time in order to compensate for the dynamic Doppler shift. In this orientation, the beam is originally red-shifted to match the initial Doppler shift and then the beam is chirped to increasingly higher frequencies in order to keep it on resonance as the atom cools. If the laser is chirped at a high enough rate then the atoms at different velocities will see an on resonance photon and can cool. Results from [13] are shown in Fig. 2.5 for a chirping experiment with varying scanning rates. Later chirping experiments resulted in stopped (and even reverse velocity) atoms [6].
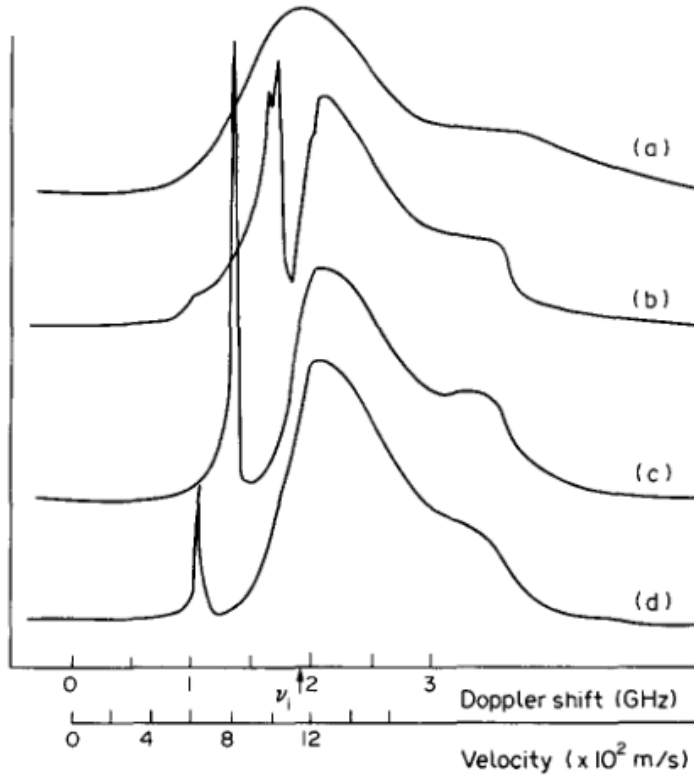
Fig. 2.5: Na atom velocity distributions for (a) no cooling laser, (b) cooling laser with no chirp, (c) chirped at 480 MHz and (d) chirped at 750 MHz. From [13].

2.5 AC Stark Light Shift

In this thesis, we present a new method for Doppler shift compensation using an energy level shift (or light shift) analogous to the Zeeman light shift. This all optical approach uses two lasers, one counter-propagating Doppler cooling and another co-propagating laser which provides an appropriate AC Stark light shift which is proportional to the intensity of the optical field which takes the role of the magnetic field in the more common Zeeman slower. This allows for comparable final

speeds (temperatures) of atoms as in the Zeeman slower but without the need for a complicated solenoid. Instead, we would need to create an appropriate inhomogeneous intensity along the path of deceleration. In later chapters two theoretical approaches to all optical cooling in an anti-resonant reflecting optical waveguide (ARROW) are described. Using ARROW structures allows us to tailor the intensity with particular design parameters and thus engineer a waveguide which could cool atoms to final speeds of $40\ m/s$ with two fixed frequency input lasers.

An expression for the AC Stark light shift can be found using second-order perturbation theory [14]. Consider a two level atom with a ground state, $|g>$ and excited state, $|e>$. If it is illuminated by a laser with wavelength $\lambda \gg r$, where r is the atom's radius, then the interaction Hamiltonian is given by $H = -\hat{\mu} \cdot \vec{E}$ (the Dipole approximation) where $\hat{\mu} = e\vec{r}$ (Dipole moment) and e is the electron charge. The resulting energy shift is given by

$$\Delta E = \mp \frac{|<e|\mu|g>|^2}{\Delta}\left|\vec{E}\right|^2 \equiv \mp \frac{\mu_{eg}^2}{\Delta}\left|\vec{E}\right|^2 \quad (2.11)$$

Where $\Delta = \delta_L - \vec{k} \cdot \vec{v}$ (equation 2.4) and $\delta_L = \omega - \omega_o$ is the detuning of the laser in the lab frame with $\hbar\omega_o = E_i$ and ω being the angular frequency of the incoming laser light. For near resonant beams, the $\mp$ signs correspond to the excited (-) and ground state (+) shifts respectively. Thus, if the light is red shifted ($\Delta < 0$) then the excited and ground states get pushed further apart. Using $I = 2\varepsilon_o c\left|\vec{E}\right|^2$ we can rewrite the light shift as

$$\Delta E = \mp \frac{\mu_{eg}{}^2 I}{2\varepsilon_o c \Delta} \quad (2.12)$$

We find that the light shift is dependent on the intensity, I of the light and inversely

proportional to the detuning from resonance, Δ.

However, atomic energy systems are of course more complicated than a

simple two level model. Alkali atom's hyperfine energy levels are often used for the

relevant energy levels in cooling experiments. In the next section, a discussion on

hyperfine energy levels in alkali atoms is described and the appropriate multi-level

AC Stark light shift is presented.

2.6 Fine and Hyperfine Structure

As electrons orbit an atomic nucleus they create a loop current and thus a

magnetic field with a resulting magnetic moment. This magnetic moment has a

corresponding orbital angular momentum, $\vec{L}$ which will couple to the electron's

intrinsic spin angular momentum, $\vec{S}$. This so called spin-orbit coupling creates a sort

of internal Zeeman splitting of the energy levels known as the fine structure with total

electron angular momentum $\vec{J} = \vec{L} + \vec{S}$. The magnitude of the total electron angular

momentum, J lies within $|L - S| \le J \le |L + S|$. Alkali atoms (which we will be

concerned with) all have one electron outside of their other filled shells. Therefore,

they act similar to hydrogen with one large core and a single orbiting electron in the

outer shell. Their ground states have $L = 0$ and $S = 1/2 = J$. The first excited state

has $L = 1$ and S$= 1/2$ leaving two possibilities for $J = 1/2, 3/2$.

Common nomenclature for the energy levels consist of the principle quantum number, L and J and the "term." For example, the ground state for the alkali Na would be written as $3^2S_{1/2}$ where the first number is the principle quantum number of the outer shell electron, the superscript is called the term and is equal to $2S' + 1$ where here $S' = \sum_i s_i$ is the sum of the spin for each electron in the system. S corresponds to the angular momentum $L = 0$ and the subscript is J. Other letters for corresponding angular momentum are $P, D, F, G \ldots = 1, 2, 3, 4$.

The hyperfine structure consists of even smaller energy spacing and are a result of the coupling between $\vec{J}$ and the total nuclear angular momentum, $\vec{I}$. The resulting total atomic angular momentum is given by $\vec{F} = \vec{J} + \vec{I}$ and has values lying within $|J - I| \leq F \leq |J + I|$. Na has $I = 3/2$, so its ground state $(L = 0, S = 1/2)$ has $F = 1, 2$. Its excited states have either $L = 0, 1$ $(3^2P_{1/2}, 3^2P_{3/2})$ and are known as the D_1 and D_2 levels and transitions respectively. The associated hyperfine transitions are $F = 1, 2$ for D_1 and $F = 0, 1, 2, 3$ for D_2. The hyperfine transitions for Na are seen in Fig. 2.6. The associated wavelengths for these transitions are 589.6 nm for D_1 and 589.2 nm for D_2 which are both easily accessible with modern lasers and are commonly used in experimental physics.

Since the hyperfine structure for an atom can consist of many closely spaced energy levels, then the simple two-level light shift derived in the previous section is not adequate. One must instead sum up the light shifts over the different unperturbed levels with the relevant detunings of the laser from each transition:

$3^2 P_{3/2}$

42.38 MHz   15.94 MHz $F = 3$

$F = 2$

50.29 MHz

66.10 MHz $F = 1$
$F = 0$

D_2 line:
589.158 nm

$3^2 P_{1/2}$ $F = 2$

70.83 MHz

118.05 MHz $F = 1$

D_1 line:
589.756 nm

$3^2 S_{1/2}$ $F = 2$

664.36 MHz

1,107.27 MHz

$F = 1$
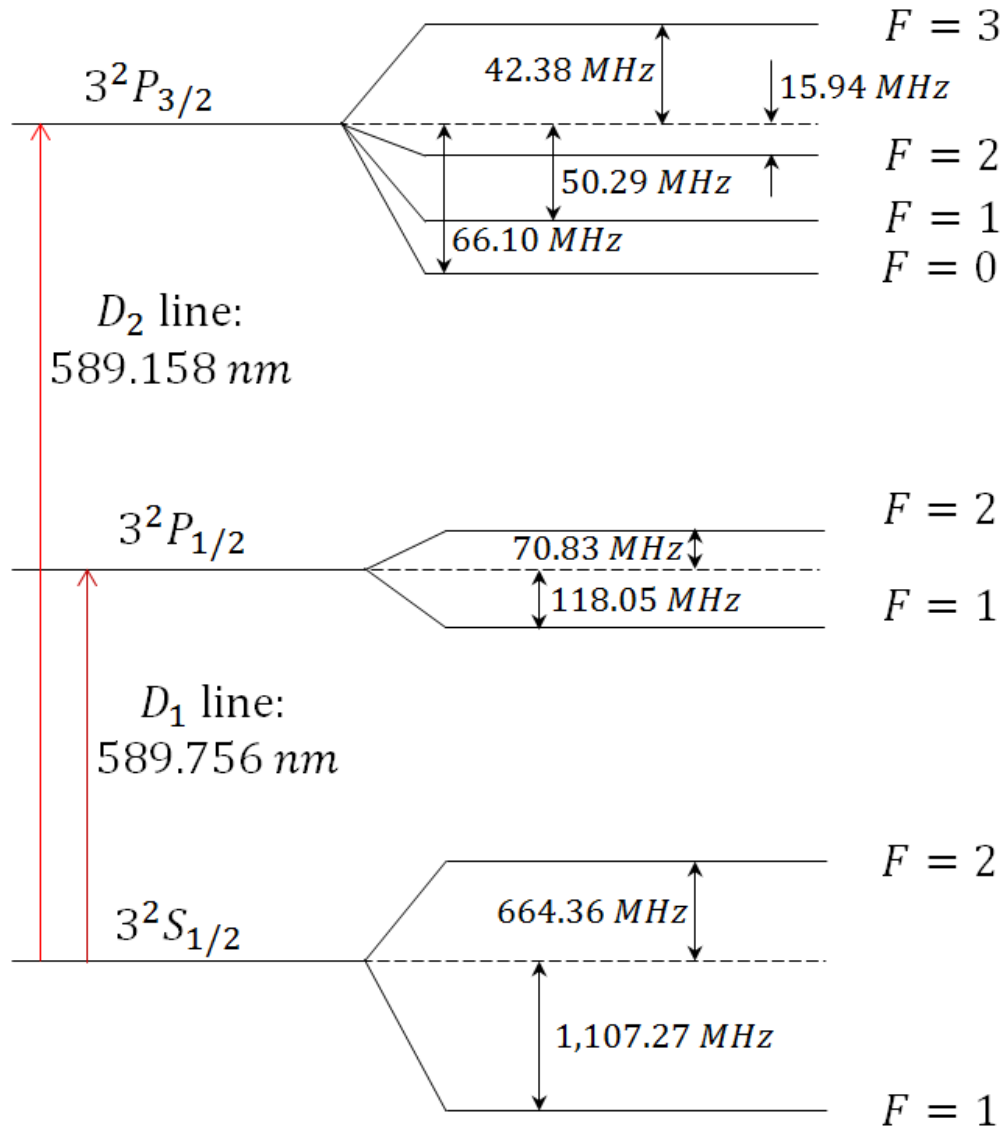
Fig. 2.6: The D_1 and D_2 hyperfine structure of Na (not drawn the scale).

$$\Delta E = \mp \frac{I}{2\varepsilon_o c} \sum_j \frac{\mu_{ij}^2}{\Delta_{ij}} \quad (2.13)$$

To make this task easier, we can consider the transition strength coefficients for the different energy levels, c_{ij}, the square of which denotes the line strengths of each transition. Using these strength transitions, the dipole moment can be re-written

as $\mu_{ij} = c_{ij}\mu_i$ (via the Wigner-Eckart Theorem [15]) where μ_i is determined by the

excited hyperfine transitions ($i = 1,2$ corresponding to $D_{1,2}$). If the detuning of the

transition is greater than the hyperfine splittings then we can approximate the ground

state energy shift by

$$\Delta E = \frac{I\mu_i^2}{2\varepsilon_o c\Delta_{F,i}} \sum c_{ij}^2 \quad (2.14)$$

Where F designates the ground state, $i = 1,2$ again designates the excited state

hyperfine level corresponding to the D_i transition and $\Delta_{F,i}$ is the detuning from the

center of the hyperfine transition to the Fth ground state. Therefore, we need only

sum over the transition strengths for a particular excited state. When the detuning of a

linearly polarized (π-polarized) laser is largely detuned ($\Delta_{F,i} \gg \Gamma_i$) then $\sum c_{ij}^2 \to \frac{1}{3}$.

All this considered, we can write the above light shift for π-polarized far detuned

light as

$$\Delta E = \frac{I\mu_i^2}{6\varepsilon_o c\Delta_{F,i}} \quad (2.15)$$

Using the relationship between dipole moment and the decay rate:

$$\Gamma_i = \frac{\omega_o^3}{3\pi\hbar\varepsilon_o c^3}\mu_i^2 \quad (2.16)$$

Where ω_o is the angular frequency for the transition, we can write the light shift as

$$\Delta E = \frac{\pi\hbar c^2\Gamma_i I}{2\omega_o^3\Delta_{F,i}} \quad (2.17)$$

2.7 Transverse Heating

Random photon emission results in heating of the atoms because as they spontaneously re-emit a photon they pick up a velocity known as a recoil velocity $\vec{v}_R = \frac{\hbar \vec{k}}{m}$. We can determine the recoil temperature T_R via the recoil energy $E_R = k_B T_R = \frac{1}{2} m v_R{}^2 = \frac{(\hbar k)^2}{2m}$. The rate at which an atom scatters a photon (thus picking up the above recoil velocity) is determined via the scattering rate (equation 2.1). There is equal probability that the photon will be emitted in one of three dimensions, therefore the probability of the recoil velocity happening in the transverse direction (not in the direction of atomic cooling) is $^2/_3$.

Such transverse speeds become non-negligible when cooling times increase. The average speed picked up in the transverse direction is $\langle v \rangle = \frac{2N v_R}{3}$. Since the final cooling velocity is typically much lower than the initial velocity we can write $\langle v \rangle = v_o - v_f \approx v_o = \sqrt{\frac{8 k_B T}{\pi m}}$. Setting these expressions equal to one another we find that $N \propto \sqrt{m}$ which we can plug back into the expression for the average speed in the transverse direction. Doing so, we find that $\langle v \rangle \propto m^{-1/2}$. Thus, the transverse heating is less of a problem for heavier atoms. Transverse heating can be ameliorated with the use of additional cooling beams (say 6 lasers, 2 counter-propagating beams for each of the 3 spatial dimensions) or via other methods (e.g. using the gradient force) as we will see in the next section.

2.8 Gradient Force

Consider the cross section of a tightly collimated Gaussian laser beam. The center of the beam contains the highest intensity and as one travels radially from the center of the beam, the intensity decreases. Therefore, the magnitude of the above described AC Stark shift will be larger in the center of the beam and will decrease in the radial direction. Also, note that the gradient force does not saturate with intensity. If the laser is detuned, then as described above, the AC Stark shift effectively changes only the ground state energy. Thus, a potential well or wall can be created within the laser beam depending on the sign of the detuning. Red-detuned light would create a potential well ($\Delta E < 0$) and blue-detuned light would result in a potential wall ($\Delta E > 0$) as seen in Fig. 2.7.a. Thus, the gradient force can be used to confine atoms to move along the direction parallel with the collimated laser and prevent transverse de-collimation if a red-shifted beam is used as seen in Fig. 2.7.b. Conversely, atoms can be pushed away from a blue-shifted beam as seen in 2.7.c [16]. One can also understand this force in the context of optically induced dipoles and it is therefore also known as the dipole force. The gradient force is very effective in waveguides due to the ability to sustain large gradients (small beam diameters) over long distances and has been used to perform atom optics experiments in waveguides as we will see in the next section.
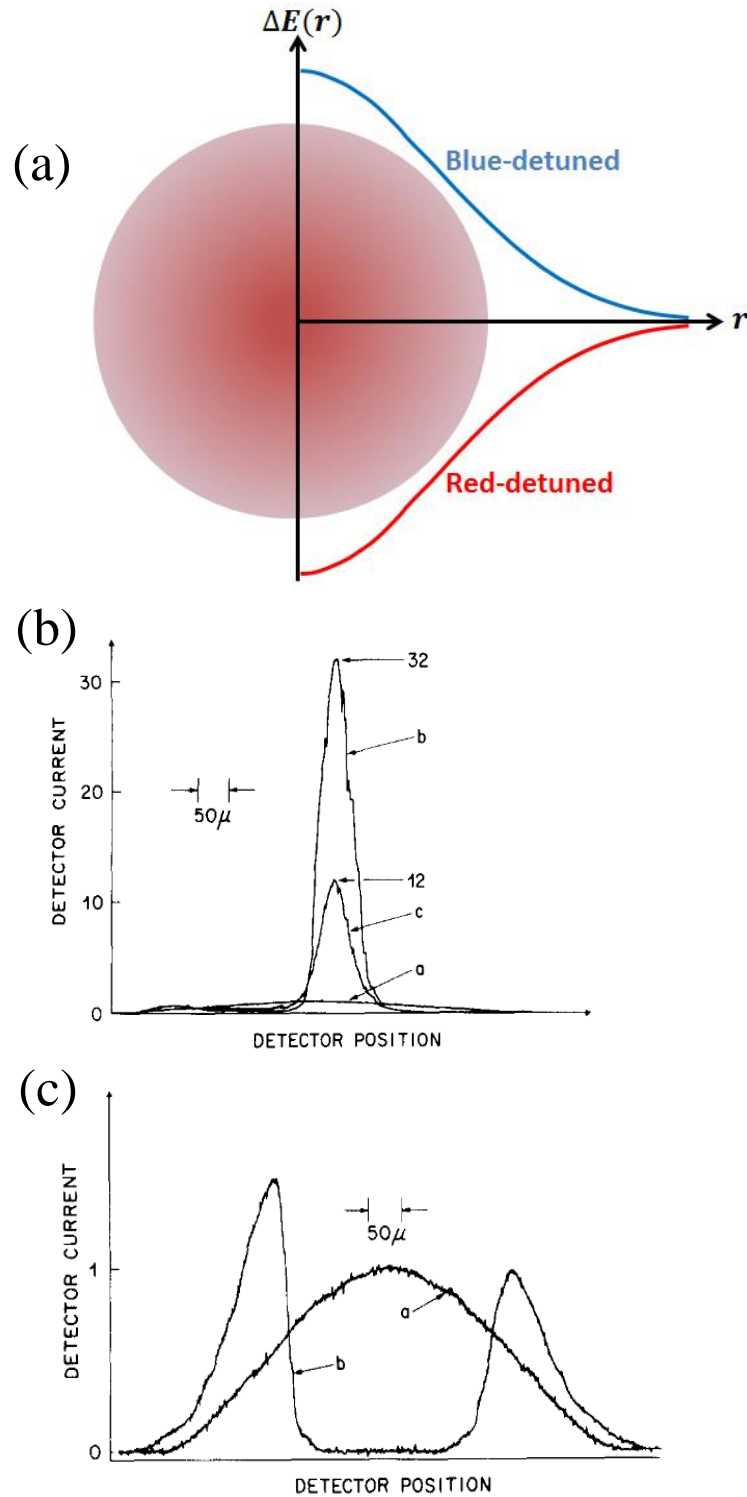
Fig. 2.7: (a) Visualization of the Gradient force for a collimated Gaussian beam. The radially dependent AC Stark shift ($\Delta E(r)$) is plotted for both the red and blue-detuned beams. (b) shows increased atomic concentration with a red detuned beam where the curves "a", "b" and "c" represent laser powers of 0, 250 and 25 mW respectively. (c) shows atomic repulsion where "a" and "b" represent a blue detuned beam with power 0 and 160 mW. (b) and (c) from [16].

2.9 Atoms in Waveguides

Hollow-core (HC) waveguides such as HC photonic crystal fiber (PCF) and HC anti-resonant reflecting optical waveguides (ARROW) have become popular platforms for guiding light in low index media. Typical atomic experiments use large glass bulk cells with dimensions on the order of centimeters. As a comparison, Fig. 2.8 shows an image of a Rubidium filled standard bulk cell of length 75 mm (Triad Technology Inc. model TT-RB87-75-V-Q) and a Rubidium filled HC-ARROW chip. Though miniaturization of atomic cells is appealing, it provides its own obstacles. Notably, atoms often stick to the walls of the cells. Since smaller cells provide the opportunity for more frequent collisions, atoms will quickly accumulate on the walls of the cell leaving it unusable after a short amount of time.

Fig. 2.8: In the upper left is a commercial bulk cell of 87Rb atoms (Triad Technology Inc.) and in the bottom right is a Rb filled HC-ARROW chip sitting on a US quarter.

Methods to prevent atoms sticking to the walls of cells include coatings (e.g. PDMS, ODMS, paraffin, etc. [17]) and using the above described gradient force [18]. Using the gradient force allows one to use an optical waveguide for light-matter experiments as the light propagates in the hollow core waveguide which doubles as

an atomic cell. If the intensity and detunings of the propagating frequencies are designed appropriately then the gradient force can provide sufficient transverse confinement to prevent unwanted collisions with the walls.

Initially proposed by Ol'Shanii et al. [19], Renn et al. were the first to optically guide Rb atoms through hollow-core fiber [18] and show that the dipole potential created by the mode profile is sufficient for transverse confinement of the atoms, producing a potential well of 71mK depth (which has a corresponding transverse capture velocity of 3.7m/s) in different size (inner diameter (ID) 40 and 10 µm) fibers. Since then, several examples of optical guiding and trapping in hollow-core photonic crystal fiber (HC-PCF) have been demonstrated [20], [21], [22], [23], [24]. Linear and nonlinear spectroscopy as well as electromagnetically induced transparency (EIT) has also been demonstrated in HC-PCF with Rb [25], [26], [27] and acetylene [28]. More recently, chip-based approaches to waveguide-based atomic spectroscopy have emerged. Our group has introduced self-contained silicon chips based on ARROWs, and demonstrated atomic spectroscopy, EIT, and slow light in Rb-filled waveguides [29][30]. Stern et al. introduced a chip platform based on evanescent fields from solid-core waveguides interacting with near-surface atoms [31].

Chapter 3

Anti-Resonant Reflecting Optical Waveguides

Here a theoretical treatment of anti-resonant reflecting optical waveguides (ARROWs) is presented. The anti-resonant condition used for guiding in low index media and the transfer matrix formalism is presented which is used for subsequent waveguide designs.

3.1 Theory

Most waveguides use total internal reflection in order to guide light. Total internal reflection uses a core medium with a higher index of refraction than the outer cladding material. The reversal of the index profile makes guiding light in low index media difficult and thus a different approach is necessary. The alkali gases that we are here interested in suffer the same problem as they have a low index of refraction ($n \cong 1$). Other low index media (e.g. water) share a similar problem though waveguides which guide in water typically result in lower loss than air/alkali cores.

Such low index guiding is achievable with interferometric confinement by structuring the high cladding index. Examples include Bragg fibers [32], photonic bandgap fibers [33] and photonic crystal slab waveguides [34]. Anti-resonant reflecting optical waveguides (ARROWs) were first proposed by Duguay [35] and

use an anti-resonance condition in order to guide leaky modes since these structures result in radiation losses as the mode propagates (finite reflectivity at each boundary). The following distinction will be made between the two types of ARROWs as follows: solid core (SC-ARROW) and hollow core (HC-ARROW). However, the anti-resonant condition is central to both.

First, we will discuss HC-ARROWs. Consider the structure found in Fig. 3.1. There is a low index core (n_c) with thickness d_c surrounded by two layers of dielectric with indices n_i and thicknesses d_i where i indicates the ith layer from the core outward. The mode wavevector, k can be decomposed into transverse components (k_T) and a component along z (β). The layers surrounding the core are each designed as Fabry-Pérot reflectors thus allowing propagation in the core.
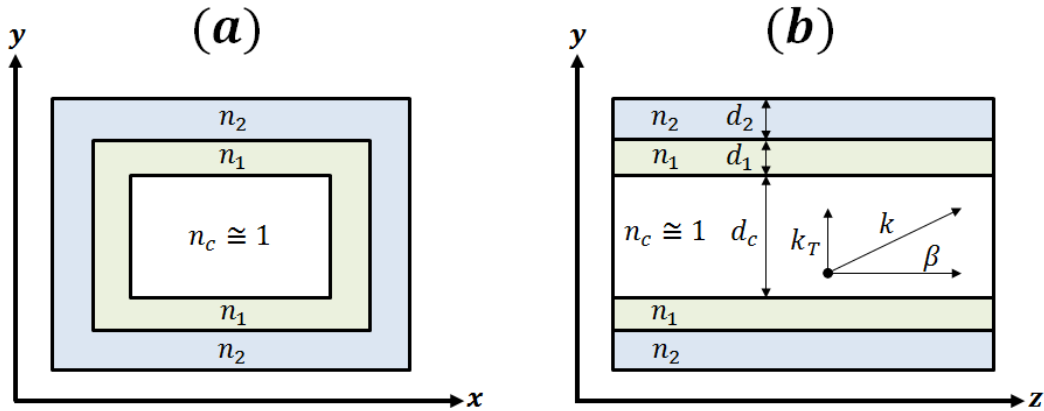

Fig. 3.1: HC-ARROW cross sections (a) in the y-x plane and (b) in the y-z plane.

The modes in an ARROWs can be either transverse electric (TE) or transverse magnetic (TM). For x-polarized light the TE mode lies in the y-direction and the TM in the x-direction. For y-polarized light the TE mode lies in the x-direction and the

TM mode in the y-direction. The anti-resonant condition is that the entire transverse

round trip phase shift is equal to an odd multiple of π. Explicitly, the condition that

needs to be satisfied in the ith layer is the following:

$$(2n - 1)\pi = 2d_i k_T + \varphi_i \quad (3.1)$$

Where $n = 1, 2, 3 \dots$ and φ_i is the total phase shift picked up at the layer boundaries.

The φ_i total phase shift needs to be carefully considered for different polarizations

and index sequences.

Consider light propagating in a material with index n_i which is incident on the

boundary with material of index n_t. Reflected TM light will acquire a π phase shift if

the incident angle is less than the Brewster angle:

$$\theta_B = \text{atan}\left(\frac{n_t}{n_i}\right) \quad (3.2)$$

TE light will acquire a π phase shift if $n_t > n_i$ and a 0 phase shift if $n_t < n_i$. The

total phase shift, φ_i in the ith layer is then the sum of the phase shifts at each of the

boundaries. For HC-ARROWs the total phase shift in the core is always $\varphi_i = 2\pi$ as

the core is a low index material. For $n_{i+1} > n_i > n_{i-1}$ the total TE phase shift is

$\varphi_i = \pi$ and for $n_i > n_{i-1}, n_{i+1}$ $\varphi_i = 0$. We use the latter index sequence for our first

ARROW layers in order to keep the same TE anti-resonance condition for all layers

as $\varphi_i = 0$ or $\varphi_i = 2\pi$ results in the condition that $2d_i k_T$ is equal to some odd integer

of π.

The total TM phase shift is more complicated as it is dependent on the

incident angle. Consider light guiding in a HC-ARROW with core index n_c with

incident angle $\theta_c = 87.4°$ on a Si_3N_4 ($n_1 = 2.1$) layer. The light refracted into the

Si_3N_4 layer will have an angle $\theta_1 = 28.4°, 39.2°$ if the core is filled with air ($n_c = 1$),

water ($n_c = 1.33$). If the next ARROW layer is made of SiO_2 ($n_2 = 1.46$) then the

Brewster angle is $\theta_{B,SiO_2} = 34.8°$ and a TM mode will acquire a phase shift of π for

air and 0 for water. The reflected light will then be incident upon the core layer again

$\theta_{B,core} = 25.5, 32.3°$ for air, water. At this boundary neither TM mode will pick up a

phase shift. Thus, for the air core waveguide we find $\varphi_{i=1} = \pi$ and for the water core

$\varphi_{i=1} = 0$ which changes the anti-resonance condition! The thickness of the ith

ARROW layer can be determined via [35]:

$$t_i = \frac{N\lambda}{4\sqrt{1 - \left(\frac{n_c}{n_i}\right)^2 + \left(\frac{\lambda}{2t_c n_i}\right)^2}}; N = \begin{cases} 1, 3, 5; \ \varphi_i = 2\pi, 0 \\ 2, 4, 6; \ \varphi_i = \pi \end{cases} \quad (3.3)$$

SC-ARROWs also use the anti-resonant condition but only on one side of the

waveguide as seen in Fig. 3.2. Since the core is made with $n > 1$ medium (typically

SiO_2), it guides via total internal reflection on the sides in which it is exposed to air.

This allows a system of solid and hollow planar waveguides to be fabricated together

on a wafer.
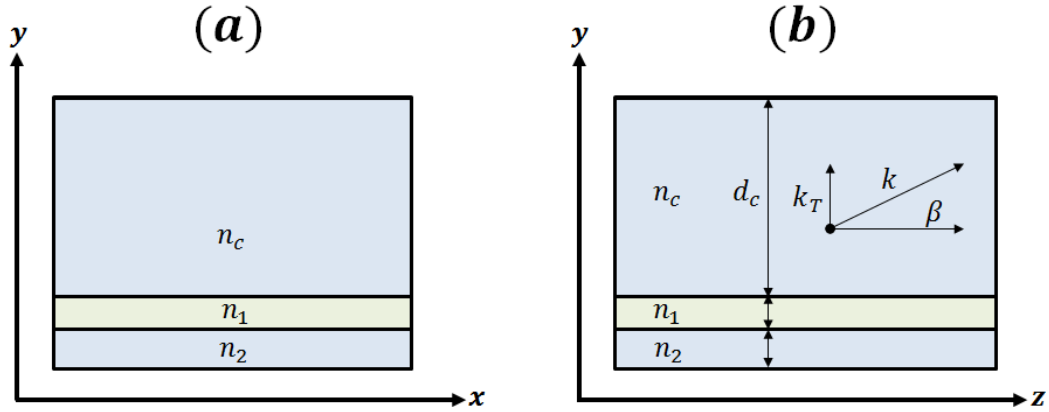
Fig. 3.2: SC-ARROW cross sections (a) in the y-x plane and (b) in the y-z plane. Light is guided in the core via the anti-resonance condition in the −y direction and via total internal reflection otherwise.

3.2 Loss

The theoretical loss in our ARROWs is calculated using a transfer matrix formalism [36]. Fig. 3.3 shows one thin layer of dielectric material in which we will examine the passage of light. Light is propagating in the positive x-direction and originates in medium 1 with index n_1. The propagating electric field can be written as

$$E(x) = Re^{-ikx} + Le^{+ikx} \equiv A(x) + B(x) \quad (3.4)$$

Where k is the wave vector in the x-direction, Re^{-ikx} is the wave traveling in the right direction and Le^{+ikx} in the left. The right and left traveling coefficients in Fig. 3.3 are defined as:

$$A_1 = A(0^-)$$

$$B_1 = B(0^-)$$

$$A'_2 = A(0^+)$$

$$B'_2 = B(0^+)$$

$$A_2 = A(x_1^-) \qquad (3.5)$$

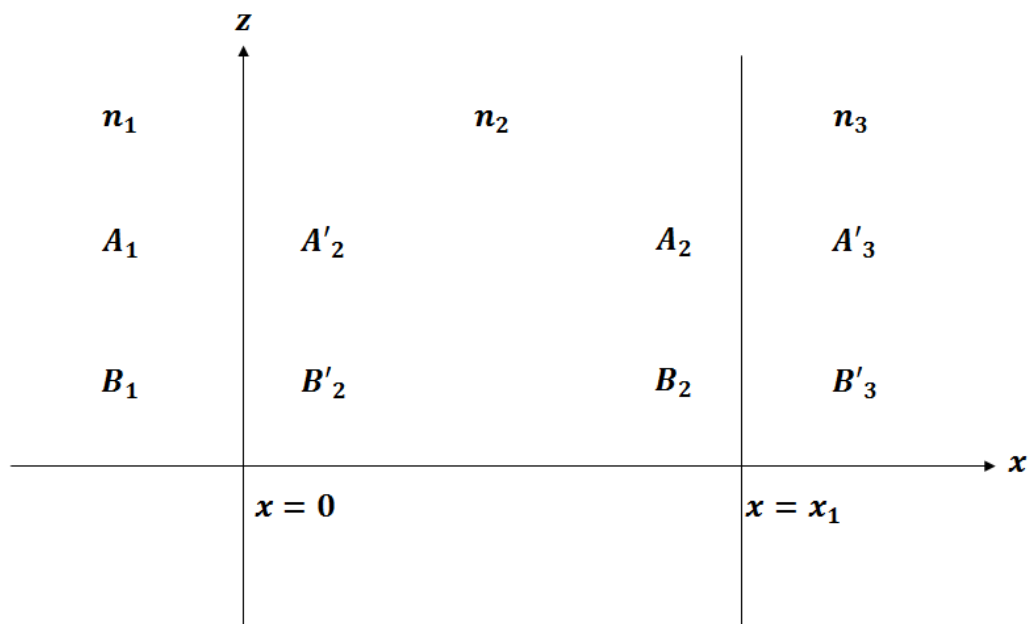$$B_2 = B(x_1^-)$$

$$A'_3 = A(x_1^+)$$

$$B'_3 = B(x_1^+)$$

Fig. 3.3: Schematic of a thin dielectric medium in which light propagates.

We desire to know the output electric field amplitudes (A'_3 and B'_3) after passing through medium 2. We can express the field amplitudes as vectors:

$$\begin{bmatrix} \begin{pmatrix} A_1 \\ B_1 \end{pmatrix} = D_1^{-1} D_2 \begin{pmatrix} A'_2 \\ B'_2 \end{pmatrix} \equiv D_{12} \begin{pmatrix} A'_2 \\ B'_2 \end{pmatrix} \\[2ex] \begin{pmatrix} A'_2 \\ B'_2 \end{pmatrix} = P_2 \begin{pmatrix} A_2 \\ B_2 \end{pmatrix} = \begin{pmatrix} e^{ik_2 x_1} & 0 \\ 0 & e^{-ik_2 x_1} \end{pmatrix} \begin{pmatrix} A'_2 \\ B'_2 \end{pmatrix} \\[2ex] \begin{pmatrix} A_2 \\ B_2 \end{pmatrix} = D_2^{-1} D_3 \begin{pmatrix} A'_3 \\ B'_3 \end{pmatrix} \equiv D_{23} \begin{pmatrix} A'_3 \\ B'_3 \end{pmatrix} \end{bmatrix} \quad (3.6)$$

Where D_i is called a dynamical matrix and is found by considering the continuity of

the electric and magnetic fields at a boundary [36]:

$$D_i = \begin{cases} \begin{pmatrix} 1 & 1 \\ n_i \cos\theta_i & -n_i \cos\theta_i \end{pmatrix} ; TE \\[2ex] \begin{pmatrix} \cos\theta_i & \cos\theta_i \\ n_i & -n_i \end{pmatrix} ; TM \end{cases} \quad (3.7)$$

P_2 adds the appropriate phase shift ($\varphi = k_2 x_1$) picked up in medium 2 where

$k_i = \dfrac{n_i \omega \cos\theta_i}{c}$. Using the above dynamical matrices, we can express the transmission

matrices, D_{ij}:

$$D_{ij} = \begin{cases} \dfrac{1}{2} \begin{pmatrix} 1 + \dfrac{k_2}{k_1} & 1 - \dfrac{k_2}{k_1} \\[2ex] 1 - \dfrac{k_2}{k_1} & 1 + \dfrac{k_2}{k_1} \end{pmatrix} ; TE \\[5ex] \dfrac{1}{2} \begin{pmatrix} 1 + \dfrac{n_2^2 k_1}{n_1^2 k_2} & 1 - \dfrac{n_2^2 k_1}{n_1^2 k_2} \\[2ex] 1 - \dfrac{n_2^2 k_1}{n_1^2 k_2} & 1 + \dfrac{n_2^2 k_1}{n_1^2 k_2} \end{pmatrix} ; TM \end{cases} \quad (3.8)$$

Therefore, we can relate the input and output field amplitudes by:

$$\begin{pmatrix} A_1 \\ B_1 \end{pmatrix} = D_1^{-1} D_2 P_2 D_2^{-1} D_3 \begin{pmatrix} A'_3 \\ B'_3 \end{pmatrix} \quad (3.9)$$

The above transfer matrix formalism can be applied to a stack of N dielectric layers

as seen in Fig. 3.4.
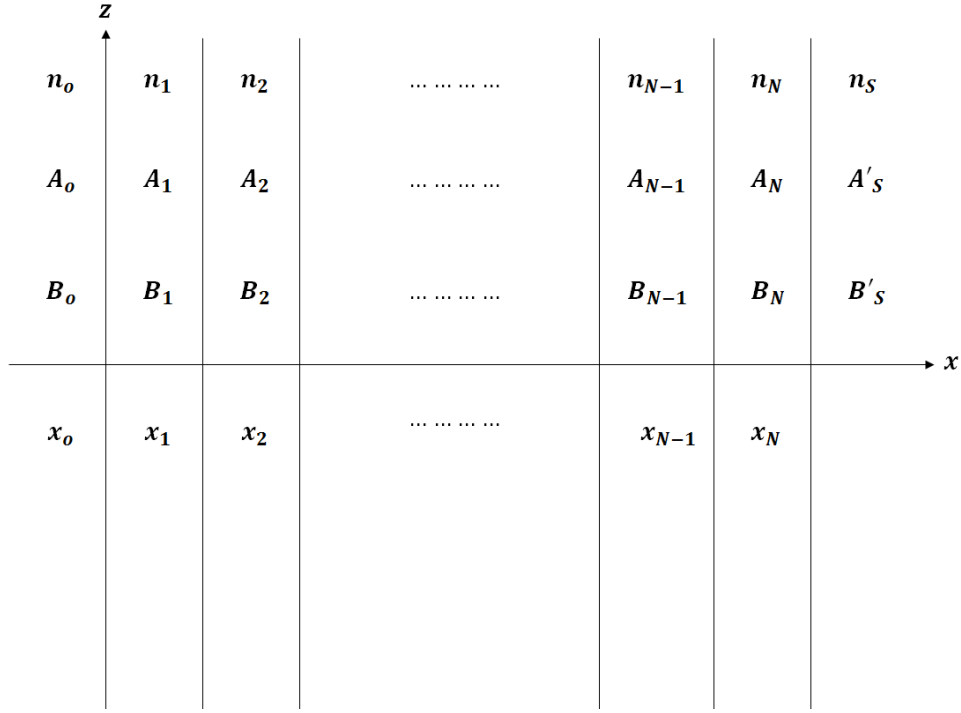
Fig. 3.4: A stack of N dielectric layers.

For the multilayer system, the relationship between the input and output field amplitudes is given by:

$$\begin{pmatrix} A_o \\ B_o \end{pmatrix} = \begin{pmatrix} M_{11} & M_{12} \\ M_{21} & M_{22} \end{pmatrix} \begin{pmatrix} A'_S \\ B'_S \end{pmatrix} \quad (3.10)$$

Where $\quad \begin{pmatrix} M_{11} & M_{12} \\ M_{21} & M_{22} \end{pmatrix} = D_o^{-1} (\prod_{i=1}^{N} D_i P_i D_i^{-1}) D_S \quad (3.11)$

Our task then is to calculate the dynamical matrices for a given structure. From this, we can calculate the reflectivity:

$$R = \left| \frac{M_{21}}{M_{11}} \right|^2 \quad (3.12)$$

The loss then is calculated as [37]:

$$\alpha = \frac{(1 - R_1 R_2)}{2 d_c \tan(\theta) \sqrt{R_1 R_2}} \quad (3.13)$$

Where R_i is the reflectivity of the ith surface, d_c is the core thickness (or width depending on what direction you are calculating the loss for) and θ is the angle of incidence from the core on the dielectric stack. Using this approach we can calculate both x and y-polarized TE and TM loss for an ARROW design. Note that in practice, fabrication imperfections and surface roughness result in a higher loss than the theoretical value. A minimum loss value has been derived for both TE and TM modes if $n_c < n_2 < n_1$:

$$\alpha_{Min\_TE} = \left(\frac{n_2{}^2 - n_c{}^2}{n_1{}^2 - n_c{}^2}\right)^{N/2} \alpha_o \quad (3.14)$$

$$\alpha_{Min\_TM} = \left(\frac{n_1{}^{N+1}}{n_2 n_c{}^N}\right)^2 \alpha_{Min_{TE}} \quad (3.15)$$

$$\alpha_o = \frac{\lambda^2 m^2}{n_c d_c{}^3 \sqrt{n_1{}^2 - n_c{}^2}} \quad (3.16)$$

Where N is the number of anti-resonant layers and $m = 1,2,3 \ldots$ is the mode order. Though these are minimum loss values, we can note several important considerations when designing an ARROW. First note that TM loss is greater than TE loss by a factor $\left(\frac{n_1{}^{N+1}}{n_2 n_c{}^N}\right)^2$. Also, loss is decreased with the addition of ARROW layers, ARROWs guide with lower loss for lower wavelengths, loss is inversely proportional to the core index and has a $d_c{}^{-3}$ dependence. For our typically fabricated HC-ARROW structures [29], we have $N = 6$ and $\lambda = 794.98\ nm$ (corresponding to the D_1 hyperfine transitions in Rubidium). Our proposed ARROW structure for atomic

cooling of Na atoms (described in the following chapter) has $N = 12$ layers at

$\lambda = 589.16 \; nm$ for low loss propagation.

Chapter 4

Atomic Slower Designs

Our aim is to engineer an ARROW which will provide an appropriate AC

Stark light shift along z in order to cool atoms all optically. As we've seen in chapter

2, ARROW structures are lossy by an amount which is very dependent on design

parameters. The loss will then determine the optical power along z and the size of the

hollow core area will determine the mode area. Therefore, for the following designs

we are concerned with engineering appropriate mode areas and losses in order to

provide the needed AC Stark shift.

Here two approaches to designing AC light shift cooling HC-ARROWs are

presented. Our aim is to cool Na atoms to final mean speeds comparable to Zeeman

slowers (tens of meters per second). As seen in Fig. 4.1 (a), two beams are used: a

counter-propagating on resonance fixed frequency Doppler cooling beam and a co-

propagating AC Stark beam in order to dynamically move the ground state and allow

for continual cooling. The relevant hyperfine transitions for Na are shown in Fig. 4.1

(b) and the detuning of the AC Stark beam from the center of the D_1 hyperfine

transitions is denoted as Δ_1. Note that in practice, the use of a re-pump beam would

be necessary to prevent population depletion for the ground state via optical pumping [5]. A brief discussion on optical pumping can be found in Appendix B. This approach is analogous to Zeeman cooling which was described in section 2.3 but instead uses the AC Stark shift which is proportional to optical intensity as described in section 2.5. We use the far detuned form of the AC Stark shift as discussed in section 2.6 (equation 2.17). The loss of the HC-ARROW is determined via the matrix formalism described in section 3.2 and is dependent on relevant design parameters. Our simulations step along the z direction and extract relevant parameters in order to satisfy the equation:
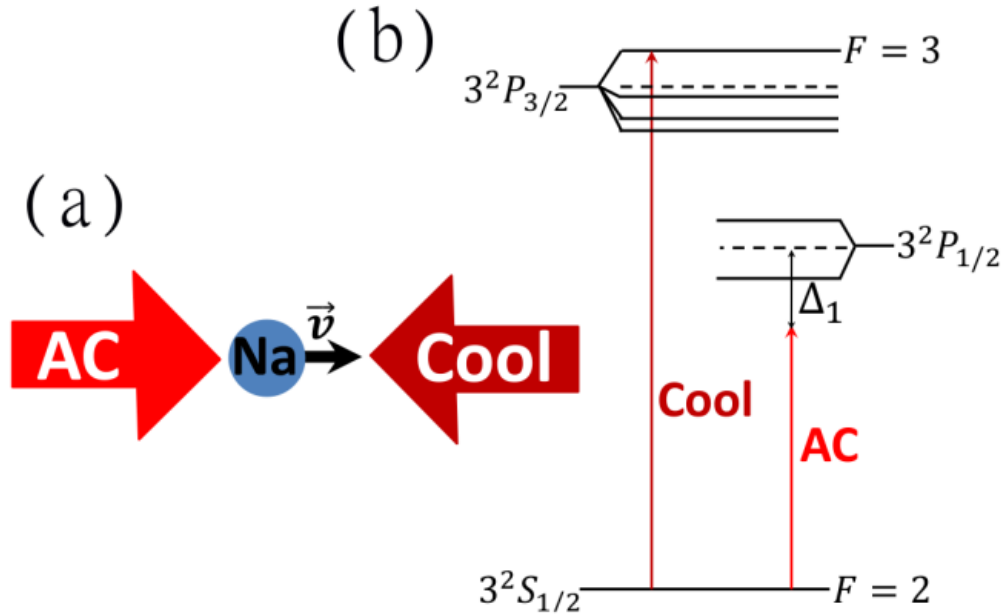
$$\Delta E_{AC}(z) + \Delta E_{D}(z) = 0 \quad (4.1)$$

Fig. 4.1: (a) Example beam geometry. Doppler "cool" beam counter-propagates while an "AC" Stark beam co-propagates with the atom. (b) The relevant hyperfine transitions for Na cooling.

The Matlab script developed for the following waveguide designs can be found in Appendix C.

4.1 Waveguide Design

For the atom we are investigating, Na, the AC Stark cooling beam is near the D_2 hyperfine transition which is 589.1583 nm. The waveguide must therefore guide at this wavelength and was designed using two oxides that we currently use to fabricate chips: SiO_2 which has an index of 1.46 and Ta_2O_5 whose index is 2.107. Our proposed waveguide consists of twelve ARROW layers as seen in Fig. 4.2 and whose thicknesses were determined from the anti-resonance condition as described in section 3.2. The hollow core has a 10 μm thickness and the width (w) varies for the following designs. From the core outward, the ARROW layers consist of alternating Ta_2O_5 (thickness 79nm) and SiO_2 (thickness 138nm) dielectrics with the exception of the final top oxide whose thickness varies in the designs below.
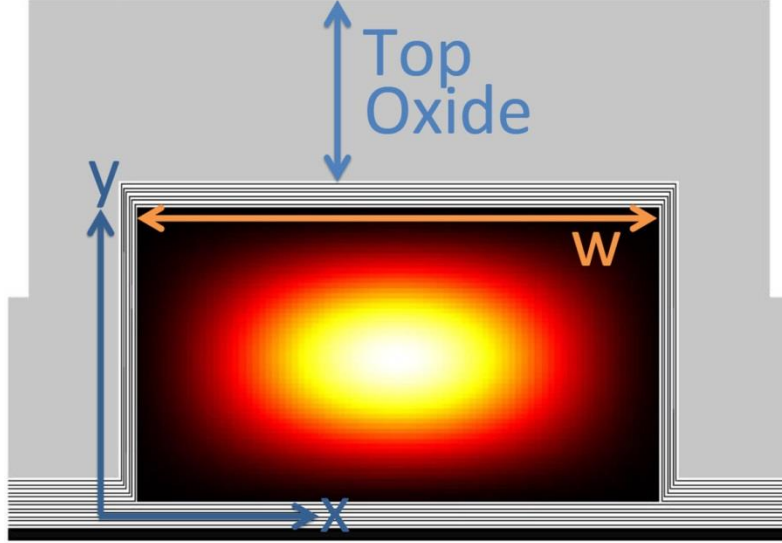
Fig. 4.2: Cross section of twelve layer HC-ARROW design. The top oxide thickness and the hollow core width, w, are the parameters to be varied in the following waveguide designs.

For continual cooling, our designs must satisfy equation 4.1 where $\Delta E_{\text{AC}}(z)$ is proportional to intensity, $I(z)$. Expressing power in a lossy waveguide along z via the Beer-Lambert law we can write:

$$I(z) = \frac{P_{\text{in}} e^{-\alpha(z)z}}{A(z)} \quad (4.2)$$

Which can be tailored by changing the loss, $\alpha(z)$, or the fundamental mode are, A(z). We can then write the AC Stark shift for our HC-ARROW using equation 4.2 combined with equation 2.17:

$$\Delta E_{AC}(z) = \frac{\pi c^2 \Gamma}{2\omega_o^3} \left(\frac{1}{\Delta_{1,F}} \right) \frac{P_{\text{in}} e^{-\alpha(z)z}}{A(z)} \quad (4.3)$$

In what remains of this chapter, we will discuss two specific approaches to implementing the new cooling scheme with Na atoms in HC-ARROW structures. In

current chip designs [29],[30] atoms are introduced into the waveguides by heating

metal reservoirs of ~2mm ID. The waveguide itself with its ~12 μm x 5 μm cross

section acts as the aperture producing a directed beam of ~3mrad divergence,

comparable to or better than previously reported examples [11], [38]. By integrating

the Maxwell thermal velocity distribution (initial temperature of 130℃) up to the

transverse capture velocity for our waveguides, we estimate guided atom fluxes on

the order of ~10^4Hz [18]. Note that though we present two ARROW based AC Stark

slowers, the experiment could in principle be performed in free space or in other

waveguides and though we propose slowing Na atoms, the methods presented here

are not limited to any particular atomic species.

4.2 Varying Width

The first example waveguide is designed by changing the width of the

waveguide along the direction of deceleration, z. Changing the width (w) will effect

both the loss and the fundamental mode area which means we need to determine

$\alpha(w)$ and $A(w)$. In order to extract these equations, a waveguide with a 10 μm core

height and varying width (between 3 and 60 μm) were simulated. The loss for each

width was determined via Matlab script which uses the previously described transfer

matrix formalism (section 2.3). The fundamental mode area was calculated using

FIMMWAVE software. These values were plotted (Fig. 4.3) and fit so that we could

then use these functions in the waveguide design simulation (appendix C.1). The fits

produced the following functions of waveguide width:

$$\alpha(w) = 0.074798 + 188.7e^{-0.68094w} \quad (4.4)$$

$$A(w) = 1.2504 + 4.383w \quad (4.5)$$

Where $\alpha(w)$ is in units cm^{-1} and $A(w)$ in μm^2. The fits are found to be good with $R > 0.998$ for both.
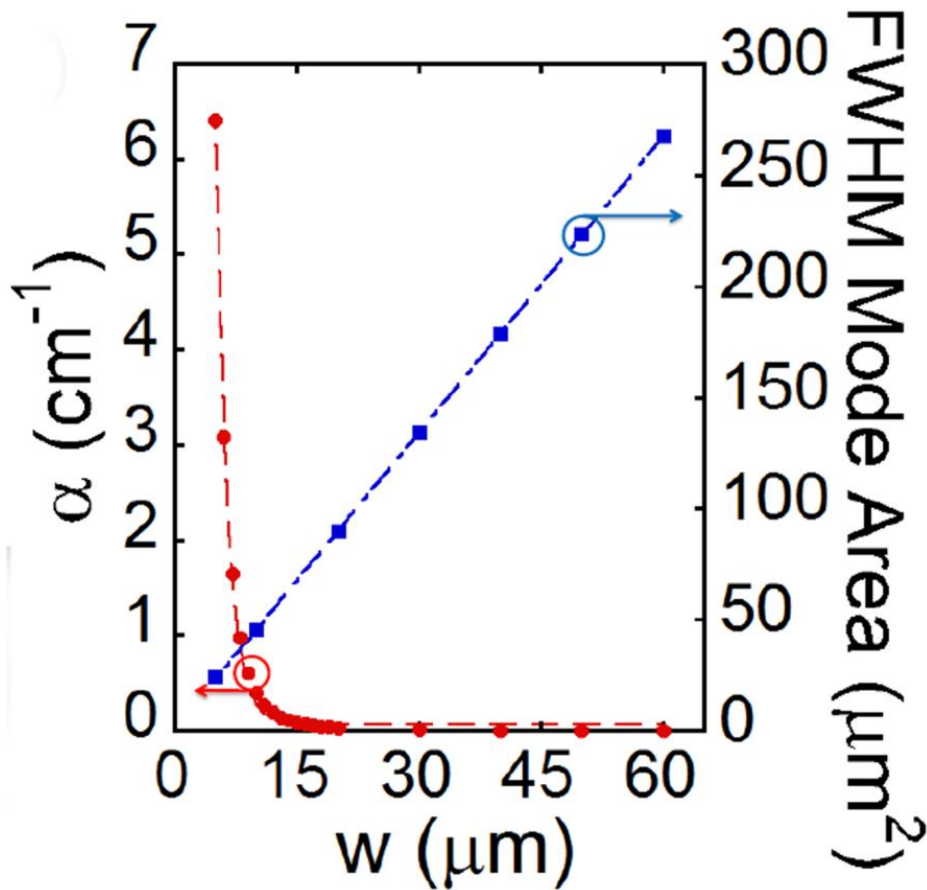

Fig. 4.3: Calculated loss and fundamental mode areas as a function of waveguide width. These results were fit and used for the simulations discussed in the text.

Using these fits and the Beer-Lambert law we can re-write equation 4.3 as a function of z and w:

$$\Delta E_{AC}(w,z) = \frac{\pi c^2 \Gamma}{2\omega_o^3}\left(\frac{1}{\Delta_{1,F}}\right)\frac{P_{in}e^{-\alpha(w)z}}{A(w)} \quad (4.6)$$

The above is then used with the Doppler shift (equation 2.5) in order to satisfy equation 4.1. To do so, we choose an initial waveguide width which determines the power input P_{in} and then solve for waveguide width at small steps along z. With appropriate initial parameters, the intensity along z can be sustained with varying width such that equation 4.1 is satisfied along the entire waveguide length (to final speed of 40 m/s). We designed such waveguides for varying initial temperatures, T_o. The waveguide designs (w vs. z) for T_o= 30, 50, 70, 90, 110 and 130℃ are plotted in Fig. 4.4 (blue, green, red, light blue, purple and gold respectively). A top down view of the waveguide can be seen in the inset of Fig. 4.4 for T_o= 50℃.
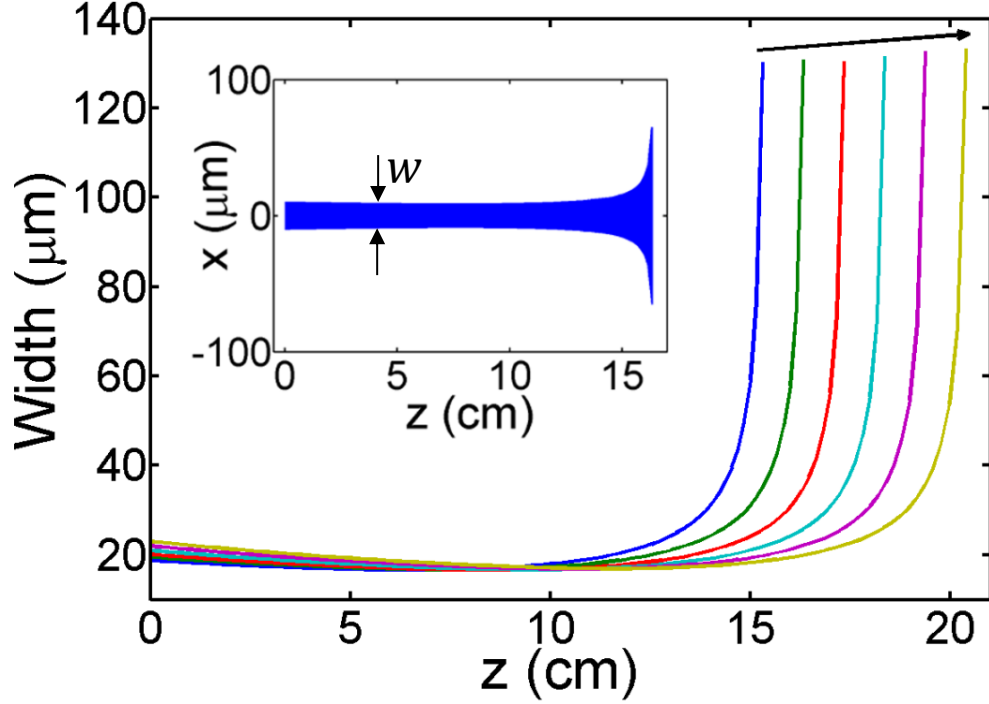
Fig. 4.4: w(z) for T_o= 30, 50, 70, 90, 110 and 130°C (blue, green, red, light blue, purple and gold respectively). Arrow indicates increasing T_o and the inset shows a top down view of the spatially varying hollow core width for $\mathbf{T_o} = 50°C$.

For $\delta_L = -8\text{GHz}$ (recall equation 2.4: $\Delta_{1,F}= \delta_L - \vec{k} \cdot \vec{v}$), P_{in} was found to be

2.59, 2.81, 3.02, 3.29, 3.58 and 3.88mW for $T_o = 30$, 50, 70, 90, 110 and 130°C,

respectively. The lengths that we considered correspond to a final temperature of

1.47K or equivalently a final mean speed $v_f = 40.0 m/s$ which is comparable to final

speeds obtained by Zeeman slowers. Notice that higher v_o requires a longer

waveguide to cool to the same v_f. Also, notice that near the end of the waveguide the

width increases dramatically which is due to the necessity to rapidly decrease

$I(z) \propto \frac{1}{A(w)}$. Lateral confinement to guard against transverse atom loss is provided by

the dipole force from the AC Stark beam as described in section 2.8. For the present mode profiles and optical powers, we calculate potential well depths on the order of 50 mK corresponding to maximum transverse capture velocities of ~6 m/s for our AC Stark beam. This provides sufficient lateral confinement along the waveguide [6].

4.3 Varying Top Oxide Thickness

The second approach is to tailor only the loss, for example by varying the thicknesses of the ARROW layers. The simplest approach is to vary one thickness, the top oxide (d_{TO}), because it is exposed post fabrication, it is the thickest layer and the loss profile is very sensitive to changes in its thickness. Using equations 2.5 and 4.3, we extract the necessary $\alpha(z)$ in order to satisfy equation 4.1 (see appendix C.2). Note that this condition with a constant mode area, A_o, allows for the derivation of an analytic expression for $\alpha(z)$:

$$\alpha(z) = \left(\frac{1}{z}\right) ln \left(\frac{-\pi c^2 \Gamma \lambda P_{in}}{2\Delta_{1,F}\omega_0^3 A_o h \sqrt{v_o^2 - 2az}}\right) \quad (4.7)$$

Fig. 4.5.a plots $\alpha(z)$ for the same range of initial temperatures for Na in a HC-ARROW with $w = 25\mu m$ and $\delta_L = -8$GHz. We are then able to design d_{TO} to the appropriate thickness along z using the transfer matrix formalism in order to achieve the desired loss.

The necessary loss coefficients to achieve $v_f = 40.0 \frac{m}{s}$ were found accessible in the range of d_{TO} between 5.98 and 6.05 μm. For $\delta_L = -8$ GHz, P_{in} was found to be 3.43, 3.59, 3.75, 3.90, 4.06 and 4.21mW for $T_o = 30, 50, 70, 90, 110$ and $130°C$

respectively. Fig. 4.5.b shows the resulting waveguide design (d_{TO} vs. z). Fig. 4.5.c plots the mean speed along z for the same initial temperatures to $v_f = 40.0 m/s$. Note that with this design procedure we are able to cool Na atoms further to their Doppler temperature, $T_D = \frac{\hbar \Gamma}{2 k_B} = 235 \ \mu K \ (v_f = 0.5 m/s)$ [10] which we were unable to achieve with the previous method due to design limitations (recall that in the previous design approach the width of the waveguide increased when approaching cooler temperatures. Therefore, in order to achieve the Doppler temperature with the varying width method, one would need a final width of unpractical size). This is the lowest temperature that we can obtain because HC-ARROWs can only guide linear polarizations over substantial lengths. This differs from free space experiments where polarization dependent sub-Doppler cooling techniques could be used to reach lower temperatures [10].
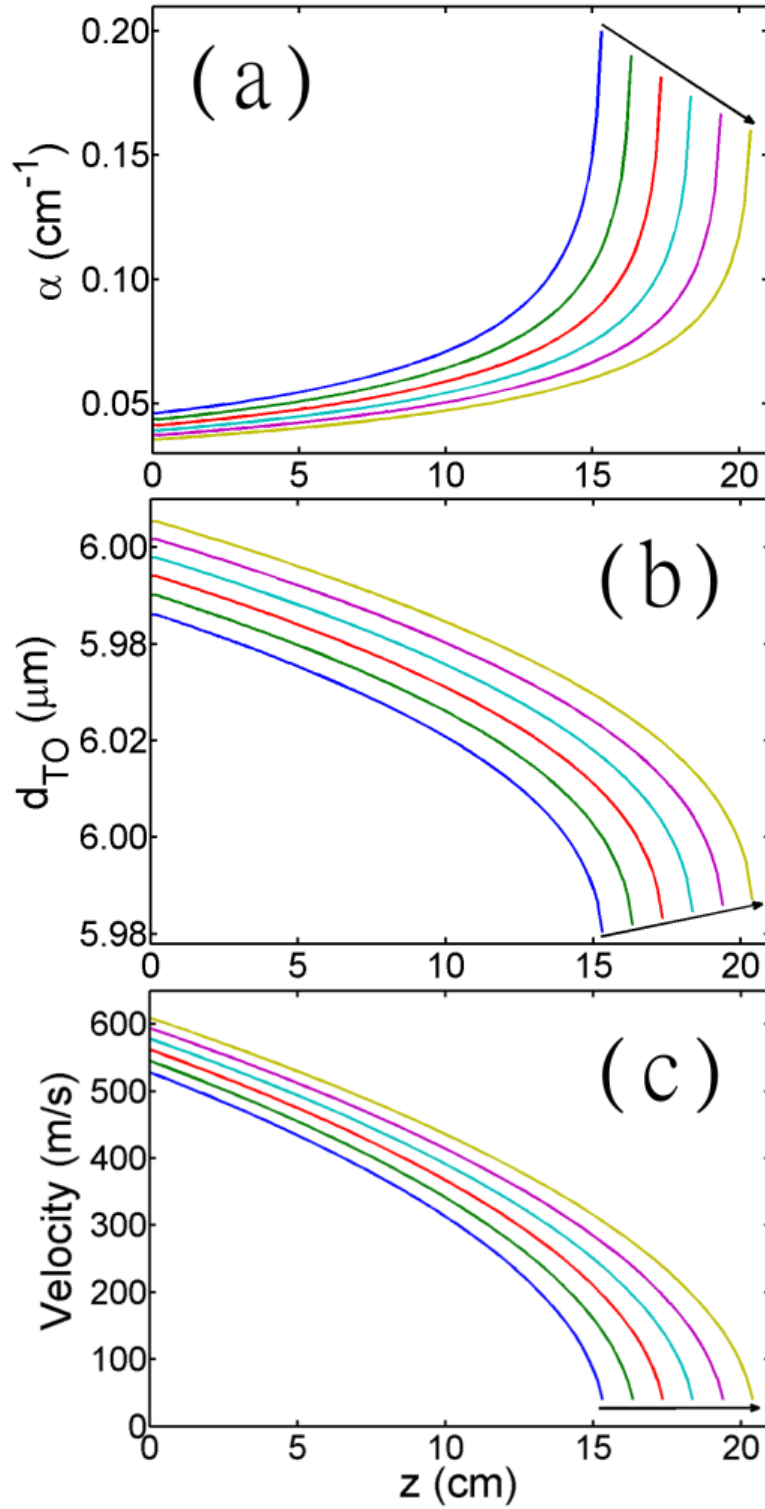
Fig. 4.5: (a) $\alpha(z)$ for T_o= 30, 50, 70, 90, 110 and 130°C (colors and arrow same as in Fig. 4.3). (b) $d_{TO}(z)$ for varying T_o. (c) $v(z)$ for varying T_o.

Chapter 5

Summary and Future Work

Here we have presented a new all optical method for cooling of atoms. Necessary theoretical framework was presented and then our AC Stark cooling approach was described. Further, we presented two designs which utilize a planar waveguide system comprised of ARROWs in order to theoretically cool Na atoms to speeds comparable to those of modern Zeeman slowers. With all optical AC Stark shift cooling, no frequency scanning is necessary and no inhomogeneous magnetic field is required, eliminating the need of a complicated solenoid.

The next steps would of course involve the realization of the proposed slower experimentally. A vision of what such an ARROW based AC Stark cooler could look like is found in Fig. 5.1. The waveguide as designed in the previous sections would lie between the Na Reservoirs. The reservoir on the top left of the drawing could be heated and the Na vapor would then co-propagate along the length of the waveguide with the AC Stark beam. The counter propagating cooling beam would be launched from the other end of the chip. Both beams could be coupled from free space or butt-coupled from fiber to a solid core waveguide on the chip. This solid core waveguide would bend around the Na reservoir and then reach the HC-ARROW where the light-matter interactions would take place. Several perpendicular SC-ARROWs could be fabricated which then intersect the HC-ARROW to collect fluorescence of the atoms

along z. Other approaches to AC Stark cooling could involve free space setups or other waveguides (e.g. hollow core photonic bandgap fiber). Also, other atoms could be used in such a cooling setup (e.g. alkalis like rubidium or cesium).
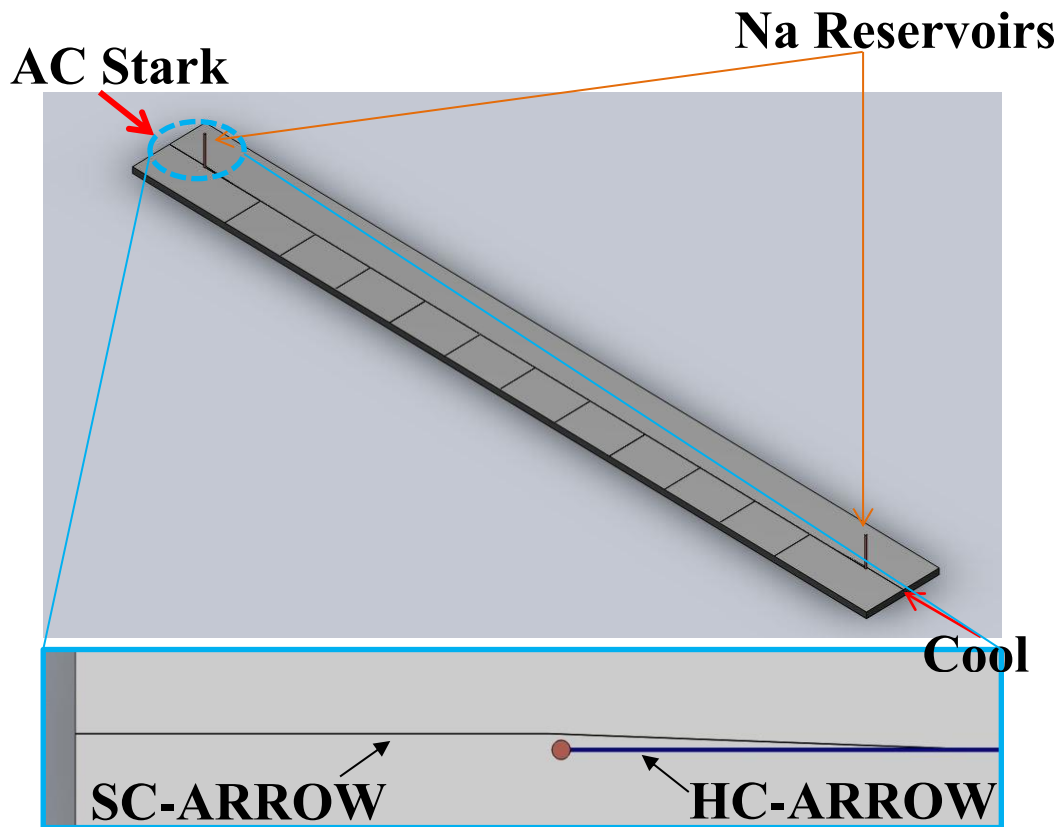
Fig. 5.1: Sketch of proposed ARROW platform AC Stark cooler. The AC Stark and Doppler cooling beams enter either side of the platform via a SC-ARROW. This waveguide bends around the Na reservoirs and leads to the HC-ARROW where the experiment takes place. Perpendicular SC-ARROWs could also be fabricated to intersect the HC-ARROW to detect fluorescence along the length of the cooler.

Appendices

Appendix A: Sodium Numbers [10]

Atomic Number		11
Atomic Mass		22.9898u 3.8175×10^{-26} kg
D$_1$	Lifetime τ	16.2992 ns
	Decay Rate (FWHM) Γ	$2\pi(9.765)$ MHz
	Wavelength λ	508.3325 nm
	Frequency ω	$2\pi(508.3325)$ THz
	Recoil Velocity v_r	2.9431 cm/s
D$_2$	Lifetime τ	16.2492 ns
	Decay Rate (FWHM) Γ	$2\pi(9.795)$ MHz
	Wavelength λ	589.1583 nm
	Frequency ω	$2\pi(508.8487)$ THz
	Recoil Velocity v_r	2.9461 cm/s

Appendix B: Optical Pumping

Optical pumping is an effect where atomic ground state polarization (accumulation of electrons in a particular energy level) is created when in the presence of laser light. Optical pumping is a non-linear light-matter interaction and can be useful or detrimental to an experiment. For instance, let us consider a two level atomic transition among fine states $J = 1$ to $J' = 0$ as seen in Fig. 2.4. Assuming there is no magnetic field present then the ground state is degenerate with magnetic sublevels $m_J = -1, 0, +1$. Before an atomic ensemble is illuminated with light, the atoms will have equally distributed ground state levels. The polarization of the light that excites an electron to the $m_J' = 0$ will determine from what ground state sublevel the electron is taken (due to selection rules).

For example, if the light is linearly polarized (π) then electrons will move from the $m_J = 0$ sublevel (selection rule $\Delta m_J = 0$) as seen in Fig. B.a and if the light is right circularly polarized (σ^+) then electrons will move from the $m_J = -1$ level (selection rule $\Delta m_J = +1$) [14] as seen in Fig. B.b. After excitation, the atoms have equal probability (the decay rate divided by three: $\frac{\Gamma}{3}$) to then decay back to either $m_J = -1, 0, +1$ ground states. Thus, after several cycles of absorption and re-emission the atoms are depleted from the sublevel connected to the excited state for a particular polarization as seen in Fig. B.c and Fig. B.d. This state is known as a dark state and the light is now allowed to pass by the atom without being absorbed. Note

that in reality there are other mechanisms which will redistribute the atoms to all of

the ground state sublevels (e.g. atomic collisions).
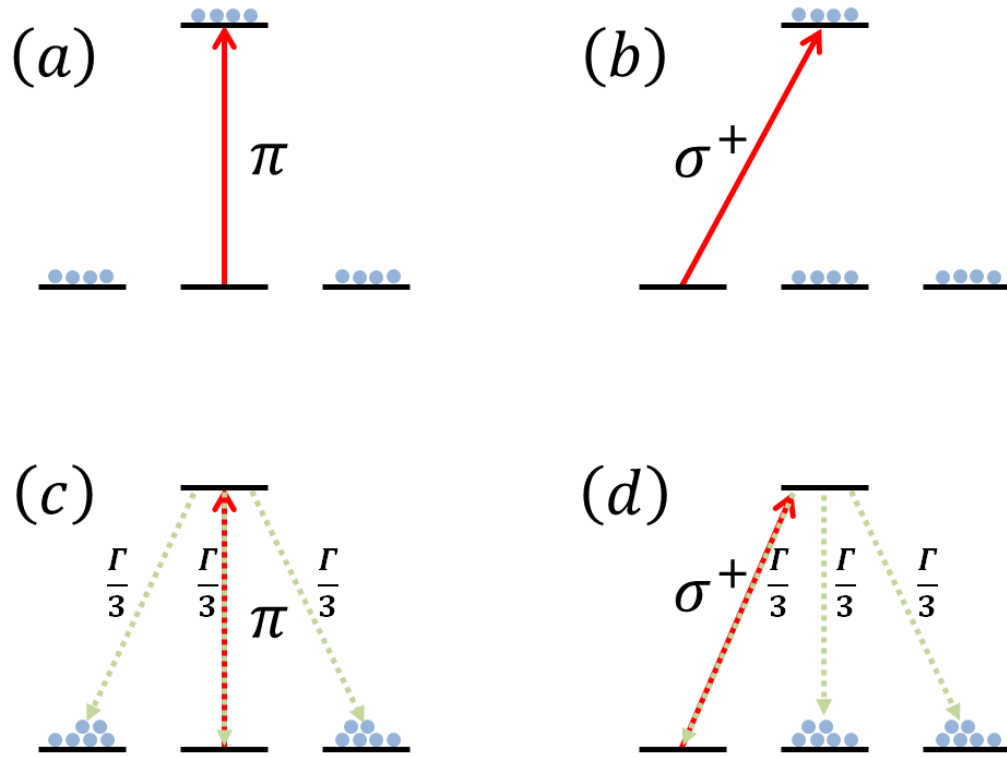
Fig. B: (a) π polarized (b) σ^+ polarized light excites an ensemble of atoms between magnetic fine sublevels according to quantum selection rules. After several cycles, the $m_J = 0, -1$ sublevel is depleted for (c) π, (d) σ^+ polarized light respectively due to the equal probability ($\frac{\Gamma}{3}$) of the atoms to relax back to any of the sublevels. This creates a so called "dark state" as the light can no longer interact with the atoms.

So we see that optical pumping can result in dark states in which the atoms

can no longer interact with incoming light. This must be carefully considered in any

optical experiment. Also, the situation is often much more complicated than the above

example. For the hyperfine atomic transitions that we are here considering, the atoms

can often decay to a lower ground state from a shared excited state. In such an

experiment, one may consider using a "re-pump" beam. This re-pump would excite the lower and excited state in order to redistribute the population to the upper ground state. Therefore, the lasers and their frequencies used for a particular experiment must be carefully chosen in any optical experiment to prevent unwanted population distribution.

In the above theoretical exercise, we considered cooling Na atoms via a Doppler cooling beam and an AC Stark beam. The relevant hyperfine transitions can be found in Fig. 4.1 (b). However, the observant reader will note that after re-emission of a photon, the atom can decay not only to the $F = 2$ ground state but also to the $F = 1$ ground state (not shown in Fig. 4.1). Therefore, a re-pump beam in the experiment would connect the $F = 1$ ground state with the D_2 $F' = 2$ excited state. This would keep the atoms from evolving into the dark state for the cooling beam (i.e. they can keep absorbing and thus cooling!). The power and detuning of this re-pumping beam would need to be properly designed to prevent loss of transverse guiding after each re-pumping event.

Appendix C: Simulation Code

C.1 Varying Width

```matlab
function [ L,dubYa,dE_aCee,dE_D,Pin,Rsquare,LAC,EacStark,diFF,Ldop]
= ACstarkNa_3( T,wO,delta2)
% AC Stark/Doppler Cooling Model
% Want to determine what sort of loss needs to be created in
waveguide in
% order to slow atoms to a stop. Inputs: T = Temp (Celcius); wO =
initial
% waveguide width, delta2 = cooling laser's detuning from D2
transition.
% T input is in Celcius, so we convert to Kelvin:
T=T+273.15;

% Acceleration = (Change in velocity from collision w/ 1
photon)/(Time
% between scattering events); tau = (hbar*2*pi)/(M*wavelength*tau) -
- m/s^2
a=-9.0643e5; %THIS IS FOR Na!

% For the stopping length!:
kb=1.3806503e-23; %Boltzman Constant! [m^2kg/Ks^2]
M=.3818e-25; %Na
v0=sqrt((8*kb*T)/(pi*M))
vF = 40; %m/s design goal: comparable to MOT cooling!
lMax=abs((((vF^2-v0^2)/(2*a))*1e2)) % [cm]


tTot=((vF-v0)/a)/1e-3

lMax=lMax*1e4; % Convert to [um]'s
deltaT=abs(((2*a*lMax*1e-6*M)/(3*kb)));
Tmin=T-deltaT;
vmin = sqrt((3*kb*Tmin)/M);
% Some values that we'll need:
hbar=1.0546e-34; %You know! [J*s]
kb=1.3806503e-23; %Boltzman Constant! [m^2kg/Ks^2]
c=3e8; %THE speed limit! [m/s]
gamma=2*pi*9.765e6; % For Na angular frequency
w0=(2*pi*c)/589.6e-9; % D2 Angular frequency of hyperfine splitting
(See Dan Steck)
NumbR=(1e12*pi*c^2*gamma)/(2*w0^3); % This is necessary to find
power in from detuning (normalized from "stuff" with given input
width);
% The 1e12 factor in NumbR is b/c Int0 will be in um^-2 and need to
convert
% to SI units at end to extract correct Pin with given detuning from
D2
```

```matlab
% lines (delta2). Delta 2 is related to the detuning from the D1
lines by a
% value deltaF (below):
Isat = 11.45*(10000/1e-3) %Saturation intensity for relevant D2 Na
transition... [W/m^2]


k=(2*pi)/589.16e-9; % k for Na D2



% TIME!::::
% t=linspace(0,180e-9);

%% Doppler Broadening:
%
% Angular frequency Difference: dW=kv (Change of apparent resonance
angular
% frequency = wave#*velocity of atom)
%
% Velocity of the atom: v=v0+at (= initial velocity +
acceleration*time)

L=linspace(0,lMax*1e-6,100); % The Doppler shift equations are in SI
units
% So we need to go back to [m]'s!
t=(-v0+sqrt(v0.^2+2*a.*L))./a;
% timeP=t(numel(t))

% THUS!
v=v0+a.*t;
% All tohhhhhgether:
dW=k.*v;
% Doppler shifted Resonant Energy:
dE_D=hbar.*dW; % [Joules]
OG=dE_D(1);
% dE_D=dE_D1.*6.24e18; % [eV]
% figure(3);plot(L.*1e2,dE_D);
% xlabel('length (cm)','FontSize',16)
% ylabel('Energy (Joules)','FontSize',16)

Ldop=L.*1e2; % Back into [cm]'s.. You know, for plots and whatnot



%% AC Stark Shift:
%%%%%%%%%%%%%%%%%%%%%%%%%%%%%%%%%%%%%%%


length = Ldop.*1e4; % The following equations require that we're in
[um]'S

w=wO;
numBr = numel(w);
wEND=w(numBr);
```

```matlab
% Loss for the waveguide design as a function of width:
alpha = 1*(0.074798 + 188.77.*exp(-0.68094.*w)); %[1/cm] WITH input
w in um's! -- Na [3] Fit = Na[2] + 10um core height

% Mode area vs. waveguide width:
Area = (1.2504 + 4.4383.*w); %[um^2]

Int0=exp(-alpha.*length.*1e-4)./Area; % [um^-2] Note: length is
multiplied by
% 1e-4 to get it from um's to cm's which we must use because alpha
is in
% 1/cm and we need the argument of exp to be unitless :) Area as
stated
% above is in um^2... Thus, this normalization factor (to be used
below)
% has the units um^-2... Need to keep this in mind for extraction of
power
% at the end of the code

stuff=-(OG.*((1/(delta2-dW(1))))^-1)/(Int0(1)); %NOTE:
stuff=(1e12*Pin*(pi*c^2*gamm)/(2*w0^3))*(2/delta2 + 1/delta1) ...
% 1e12 prefactor is due to Int0 being in units of um^-3, not SI
units...

%
figure(2);plot(LAC,EacStark./(1e9*hbar),'r',Ldop,dE_D./(1e9*hbar),'b
');
% xlabel('length (cm)','FontSize',16);
% ylabel('Detuning (GHz)','FontSize',16)

%% Fitting for width along the direction of deceleration:
L=length.*1e-4;

Width=linspace(20,5);
endvalW=numel(Width);
endvalL=numel(L);

DiF=1e-24;
for i=1:endvalL
    lL=L(i);

fitAC=@(varz)(abs(dE_D(i)+stuff.*((1./(delta2-dW(i)))).*exp( -
(0.074798 + 188.77.*exp(-0.68094.*varz(1))).*lL )./ ((1.2504 +
4.4383.*varz(1))))));
guess=[30];
options=optimset('TolX',0.1e-25);
dubYa(i) = fminsearch(fitAC,guess,options);

end
    figure(42); plot(L,dubYa./2,'b',L,-dubYa./2,'b');
    xlabel('length (cm)','FontSize',16);
```

```matlab
    ylabel('Design (\mum)','FontSize',16)

    endWidth=dubYa(numel(dubYa))

    dE_aCee=(stuff.*((1./(delta2-dW))).*exp( -(0.074798 +
188.77.*exp(-0.68094.*dubYa)).*L ))./ ((1.2504 + 4.4383.*dubYa));
%    figure(5); plot(L,dE_aCee,'r-*',L,-dE_D,'b')
    Pin=(stuff/NumbR)*1e3


%%%%%%%%%%%%%%%%%%%%%%%%%%%%%%%%%%%%%%%%%%%%%%%%%%%%%%%%%%%%%%%%%%
%%%%%%%%%%%%%%%%%%%%%%%%%%%%%%%%%%%%%%%%%%%%%%
%%%%%%%%%%%%%%%%%%%%%%%%%%%%%% Potential Well
%%%%%%%%%%%%%%%%%%%%%%%%%%%%%%
%%%%%%%%%%%%%%%%%%%%%%%%%%%%%%%%%%%%%%%%%%%%%%%%%%%%%%%%%%%%%%%%%%
%
% WellTemp=(dE_aCee./1.3806488e-23)./1e-3; % This is the energy
shift/boltzmann const in J/K. Temp in mK!!!
% % This will give a potential well depth in Kelvin! Renn et al PRL
75, 18 (1995)
%
%
% Fin=numel(WellTemp);
% GuideTimMin=abs(dE_aCee(Fin)*2*M)/(hbar^2*k^2*(gamma/2)) % This is
the diffusion time for a given
% % Potential well.
%
% FWHM=13.294; %From FIMMWAVE FWHM mode [um]
% ce=FWHM/(2*sqrt(2*log(2))); %Convert to std dev for Gaussian
function below
% Rfin=25/2;
%
% R=linspace(0,Rfin);
%
% NormG=exp(-(R.^2)./(2*ce^2));
%
% for i=1:numel(L)
%
% RadWell(i,:)=WellTemp(i).*NormG;
% end
%
% figure(99);mesh(R,L,RadWell)

Uac=(dE_aCee./1.3806488e-23).*1e3; % This is the energy
shift/boltzmann const in J/K. Temp in mK!!!
Ud=(WELL(Isat,dW/(2*pi),589.16e-9,gamma/(2*pi)))*1e3; % Potential
well from doppler cooling beam at saturation intensity in mK
Utot=Uac+Ud;

figure(111);plot(L,Uac)
%
% figure(8);plot(L,WellTemp)
```

```
%      xlabel('Length (cm)','FontSize',16);
%      ylabel('Potential Depth (mK)','FontSize',16)

% vTmax=sqrt((2.*abs(dE_aCee))./M);
% figure(9);plot(L,vTmax);
%      xlabel('Length (cm)','FontSize',16);
%      ylabel('Max Transverse Capture Velocity (m/s)','FontSize',16)

% DIFF = abs(dE_aCee - dE_D);
% figure(17); plot(L,DIFF);
%      xlabel('Length (cm)','FontSize',16);
%      ylabel('\delta(\DeltaE) (MHz)','FontSize',16)

end
```

C.2 Varying Top Oxide Thickness

```
function [ Ldop,TOthick,dE_D,dEac,alpha ] = NaSlowerConstantW( T,w )
% AC Stark/Doppler Cooling Model
% Want to determine what sort of loss needs to be created in
waveguide in
% order to slow atoms to a stop. Inputs: T = Temp (Celcius); w =
width (um)
% T input is in Celcius, so we convert to Kelvin:
T=T+273.15;
Area = (1.2504 + 4.4383.*w); %[um^2]
alpha = 1*(0.074798 + 188.77.*exp(-0.68094.*w)); %[1/cm] WITH input
w in um's! -- Na [3] Fit = Na[2] + 10um core height
Int0=exp(-alpha.*0.*1e-4)./Area;


% For the stopping length!:
kb=1.3806503e-23; %Boltzman Constant! [m^2kg/Ks^2]
M=.3818e-25; %Na
v0=sqrt((8*kb*T)/(pi*M));
a=-9.0643e5; %THIS IS FOR Na!
Td=235e-6; %Doppler temp in K
vF=40; % 40m/s final velocity goal (for paper)
vfinal = vF;
lMax=abs(((vfinal^2-v0^2)/(2*a))*1e2); % [cm] = max length
considered (input vfinal = vd or vF for desired final velocity)

lMax=lMax*1e4; % Convert to [um]'s
deltaT=abs(((2*a*lMax*1e-6*M)/(3*kb)));
Tmin=T-deltaT;
% Some values that we'll need:
hbar=1.0546e-34; %You know! [J*s]
kb=1.3806503e-23; %Boltzman Constant! [m^2kg/Ks^2]
```

53

```matlab
c=3e8; %THE speed limit! [m/s]
gamma=2*pi*9.765e6; % For Cs
w0=(2*pi*c)/589.16e-9; % D2: Angular frequency of hyperfine
splitting (See Dan Steck)
NumbR=(1e12*pi*c^2*gamma)/(2*w0^3); % This is necessary to find
power in from detuning (normalized from "stuff" with given input
width);
% The 1e12 factor in NumbR is b/c Int0 will be in um^-2 and need to
convert
% to SI units at end to extract correct Pin with given detuning from
D2
% lines (delta2). Delta 2 is related to the detuning from the D1
lines by a
% value deltaF (below):
deltaF=0.517e12; % Detuing between D1 and D2 fine splitting in Na
(See Dan Steck);


k=(2*pi)/589.16e-9; % k for CS D2



% TIME!::::
% t=linspace(0,180e-9);

%% Doppler Broadening:
%
% Angular frequency Difference: dW=kv (Change of apparent resonance
angular
% frequency = wave#*velocity of atom)
%
% Velocity of the atom: v=v0+at (= initial velocity +
acceleration*time)

%
% Acceleration = (Change in velocity from collision w/ 1
photon)/(Time
% between scattering events); tau = (hbar*2*pi)/(M*wavelength*tau) -
- m/s^2
a=-9.0643e5; %THIS IS FOR Na!

L=linspace(0,lMax*1e-6,100); % The Doppler shift equations are in SI
units
% So we need to go back to [m]'s!
t=(-v0+sqrt(v0.^2+2*a.*L))./a;
% THUS!
v=v0+a.*t;
% All tohhhhgether:
dW=k.*v;
% Doppler shifted Resonant Energy:
dE_D=hbar.*dW; % [Joules]
endval=numel(dE_D);
% dE_D=dE_D1.*6.24e18; % [eV]
% figure(3);plot(L.*1e2,dE_D);
```

```matlab
% xlabel('length (cm)','FontSize',16)
% ylabel('Energy (Joules)','FontSize',16)


[p,S] = polyfit((L),dE_D,1);
Output = polyval(p,(L));
slopeDoppler=p(1);
intDoppler=p(2);
OG=dE_D(1);

delta2=-8e9;
stuff=-(OG.*((1/(delta2-dW(1))))^-1)/(Int0(1)); %NOTE:
stuff=(1e12*Pin*(pi*c^2*gamm)/(2*w0^3))*(2/delta2 + 1/delta1) ...
1e12 prefactor is due to Int0 being in
% units of um^-3, not SI units...
Ldop=L.*1e2; % Back into [cm]'s.. You know, for plots and whatnot

%% AC Stark: Calculate alpha as a function of length with a given
width
L=Ldop;

endvalL=numel(L);

DiF=1e-24;
for i=2:endvalL
    lL=L(i);

fitAC=@(varz)(abs(dE_D(i)+((stuff.*((1./(delta2-dW(i)))).*exp( -
varz(1).*lL ))./ (Area))));
guess=[.30];
options=optimset('TolX',0.1e-25);
alpha(i) = fminsearch(fitAC,guess,options);

end
alpha(1)=alpha(2);
figure(1); plot(Ldop,alpha)
xlabel('length (cm)','FontSize',16)
ylabel('\alpha (1/cm)','FontSize',16)

[TopO,AlphaSim]=AlphaVsTOthickness(5.9535,6.155,w);
endvalA=numel(alpha);

for i=1:endvalA
    diff = abs(AlphaSim-alpha(i));
    [minZ,INdZ]=min(diff);

    TOthick(i)=TopO(INdZ);
    MinZs(i)=minZ;
end

dEac=(stuff.*((1./(delta2-dW))).*exp(-alpha.*Ldop))./Area;
```

```matlab
DIFF = abs(dEac - dE_D);
figure(4); plot(Ldop,-dE_D,'r',Ldop,dEac,'*-b');

figure(2); plot(Ldop,TOthick);
xlabel('length (cm)','FontSize',16)
ylabel('Top Oxide Thickness (um)','FontSize',16)

% figure(3); plot(Ldop,MinZs);
% xlabel('length (cm)','FontSize',16)
% ylabel('Difference in \alpha','FontSize',16)

% figure(5); plot(Ldop,DIFF./1e6);
%     xlabel('Length (cm)','FontSize',16);
%     ylabel('\delta(\DeltaE) (MHz)','FontSize',16)

    delta2=-8e9;
    deltaF=0.517e12;
    NumbR=(1e12*pi*c^2*gamma)/(2*w0^3);
    Pin=(stuff/NumbR)*1e3


    WellTemp=(dEac./1.3806488e-23)./1e-3; % This is the energy
shift/boltzmann const in J/K. Temp in mK!!!
% This will give a potential well depth in Kelvin! Renn et al PRL
75, 18 (1995)
initialPotWell=WellTemp(1);

% figure(23);plot(L,WellTemp)

Fin=numel(WellTemp);
GuideTimMin=abs(dEac(Fin)*2*M)/(hbar^2*k^2*(gamma/2));

FWHM=13.294; %From FIMMWAVE FWHM mode [um]
ce=FWHM/(2*sqrt(2*log(2))); %Convert to std dev for Gaussian
function below
Rfin=25/2;

R=linspace(0,Rfin);

NormG=exp(-(R.^2)./(2*ce^2));

for i=1:numel(L)

RadWell(i,:)=WellTemp(i).*NormG;
end
% figure(99);mesh(R,L,RadWell)
end
```

Bibliography

[1]   J. A. Black and H. Schmidt, "Atomic cooling via AC Stark shift," *Opt. Lett.*, vol. 39, no. 3, pp. 536–539, Feb. 2014.

[2]   A. Ashkin, "Acceleration and Trapping of Particles by Radiation Pressure," *Phys. Rev. Lett.*, vol. 24, no. 4, pp. 156–159, Jan. 1970.

[3]   A. Ashkin, "Atomic-beam deflection by resonance-radiation pressure," *Phys. Rev. Lett.*, vol. 25, no. 19, pp. 1321–1324, 1970.

[4]   T. W. Hänsch and A. L. Schawlow, "Cooling of gases by laser radiation," *Opt. Commun.*, vol. 13, no. 1, pp. 68–69, Jan. 1975.

[5]   W. D. Phillips, "Nobel Lecture: Laser cooling and trapping of neutral atoms," *Rev. Mod. Phys.*, vol. 70, no. 3, pp. 721–741, Jul. 1998.

[6]   W. Ertmer, R. Blatt, J. L. Hall, and M. Zhu, "Laser Manipulation of Atomic Beam Velocities: Demonstration of Stopped Atoms and Velocity Reversal," *Phys. Rev. Lett.*, vol. 54, no. 10, pp. 996–999, Mar. 1985.

[7]   J. Prodan, A. Migdall, W. D. Phillips, I. So, H. Metcalf, and J. Dalibard, "Stopping Atoms with Laser Light," *Phys. Rev. Lett.*, vol. 54, no. 10, pp. 992–995, Mar. 1985.

[8]   C. J. Dedman, J. Nes, T. M. Hanna, R. G. Dall, K. G. H. Baldwin, and A. G. Truscott, "Optimum design and construction of a Zeeman slower for use with a magneto-optic trap," *Rev. Sci. Instrum.*, vol. 75, no. 12, pp. 5136–5142, Nov. 2004.

[9]   R. Grimm, M. Weidemüller, and Y. B. Ovchinnikov, "Optical dipole traps for neutral atoms," *arXiv:physics/9902072*, Feb. 1999.

[10]   W. D. Phillips and H. Metcalf, "Laser deceleration of an atomic beam," *Phys. Rev. Lett.*, vol. 48, no. 9, pp. 596–599, 1982.

[11]   D. Steck, "Alkali D Line Data." 2010.

[12]   K. J. Gunter, "Design and implementation of a Zeeman slower for 87Rb," Ecole Normale Superieure, Paris, 2004.

[13]   J. V. Prodan and W. D. Phillips, "Chirping the light—fantastic? Recent NBS atom cooling experiments," *Prog. Quantum Electron.*, vol. 8, no. 3–4, pp. 231–235, 1984.

[14]   M. Auzinsh, D. Budker and S.M. Rochester, *Optically Polarized Atoms*, 1st ed. Oxford University Press, 2010.

[15]   R. Shankar, *Principles of Quantum Mechanics*, Second. Springer.

[16]   D. B. Pearson, R. R. Freeman, J. E. Bjorkholm, and A. Ashkin, "Focusing and defocusing of neutral atomic beams using resonance-radiation pressure," *Appl. Phys. Lett.*, vol. 36, no. 1, pp. 99–101, 1980.

[17]   A. R. Bhagwat and A. L. Gaeta, "Nonlinear optics in hollow-core photonic bandgap fibers," *Opt. Express*, vol. 16, no. 7, pp. 5035–5047, Mar. 2008.

[18]   M. J. Renn, D. Montgomery, O. Vdovin, D. Z. Anderson, C. E. Wieman, and E. A. Cornell, "Laser-Guided Atoms in Hollow-Core Optical Fibers," *Phys. Rev. Lett.*, vol. 75, no. 18, pp. 3253–3256, Oct. 1995.

[19]   M. A. Ol'Shanii, Y. B. Ovchinnikov, and V. S. Letokhov, "Laser guiding of atoms in a hollow optical fiber," *Opt. Commun.*, vol. 98, no. 1–3, pp. 77–79, Apr. 1993.

[20]   C. A. Christensen, S. Will, M. Saba, G.-B. Jo, Y.-I. Shin, W. Ketterle, and D. Pritchard, "Trapping of ultracold atoms in a hollow-core photonic crystal fiber," *Phys. Rev. A*, vol. 78, no. 3, p. 033429, Sep. 2008.

[21]   M. Bajcsy, S. Hofferberth, V. Balic, T. Peyronel, M. Hafezi, A. S. Zibrov, V. Vuletic, and M. D. Lukin, "Efficient All-Optical Switching Using Slow Light within a Hollow Fiber," *Phys. Rev. Lett.*, vol. 102, no. 20, p. 203902, May 2009.

[22]   T. Takekoshi and R. J. Knize, "Optical Guiding of Atoms through a Hollow-Core Photonic Band-Gap Fiber," *Phys. Rev. Lett.*, vol. 98, no. 21, p. 210404, May 2007.

[23]   M. J. Renn, E. A. Donley, E. A. Cornell, C. E. Wieman, and D. Z. Anderson, "Evanescent-wave guiding of atoms in hollow optical fibers," *Phys. Rev. A*, vol. 53, no. 2, pp. R648–R651, Feb. 1996.

[24]   H. Ito, T. Nakata, K. Sakaki, M. Ohtsu, K. I. Lee, and W. Jhe, "Laser Spectroscopy of Atoms Guided by Evanescent Waves in Micron-Sized Hollow Optical Fibers," *Phys. Rev. Lett.*, vol. 76, no. 24, pp. 4500–4503, Jun. 1996.

[25]   P. S. Light, F. Benabid, F. Couny, M. Maric, and A. N. Luiten, "Electromagnetically induced transparency in Rb-filled coated hollow-core photonic crystal fiber," *Opt. Lett.*, vol. 32, no. 10, pp. 1323–1325, May 2007.

[26]   A. D. Slepkov, A. R. Bhagwat, V. Venkataraman, P. Londero, and A. L. Gaeta, "Spectroscopy of Rb atoms in hollow-core fibers," *Phys. Rev. A*, vol. 81, no. 5, p. 053825, May 2010.

[27]   V. Venkataraman, P. Londero, A. R. Bhagwat, A. D. Slepkov, and A. L. Gaeta, "All-optical modulation of four-wave mixing in an Rb-filled photonic bandgap fiber," *Opt. Lett.*, vol. 35, no. 13, pp. 2287–2289, Jul. 2010.

[28]   P. S. Light, F. Benabid, G. J. Pearce, F. Couny, and D. M. Bird, "Electromagnetically induced transparency in acetylene molecules with counterpropagating beams in V and Λ schemes," *Appl. Phys. Lett.*, vol. 94, no. 14, p. 141103, Apr. 2009.

[29]   W. Yang, D. B. Conkey, B. Wu, D. Yin, A. R. Hawkins, and H. Schmidt, "Atomic spectroscopy on a chip," *Nat. Photonics*, vol. 1, no. 6, pp. 331–335, Jun. 2007.

[30]   B. Wu, J. F. Hulbert, E. J. Lunt, K. Hurd, A. R. Hawkins, and H. Schmidt, "Slow light on a chip via atomic quantum state control," *Nat. Photonics*, vol. 4, no. 11, pp. 776–779, Nov. 2010.

[31]   L. Stern, B. Desiatov, I. Goykhman, and U. Levy, "Nanoscale light–matter interactions in atomic cladding waveguides," *Nat. Commun.*, vol. 4, p. 1548, Mar. 2013.

[32]   P. Yeh, A. Yariv, and C.-S. Hong, "Electromagnetic propagation in periodic stratified media. I. General theory," *J. Opt. Soc. Am.*, vol. 67, no. 4, pp. 423–438, Apr. 1977.

[33]   J. C. Knight, T. A. Birks, P. S. J. Russell, and D. M. Atkin, "All-silica single-mode optical fiber with photonic crystal cladding," *Opt. Lett.*, vol. 21, no. 19, pp. 1547–1549, Oct. 1996.

[34]   S. G. Johnson, P. R. Villeneuve, S. Fan, and J. D. Joannopoulos, "Linear waveguides in photonic-crystal slabs," *Phys. Rev. B*, vol. 62, no. 12, pp. 8212–8222, Sep. 2000.

[35]   M. A. Duguay, Y. Kokubun, T. L. Koch, and L. Pfeiffer, "Antiresonant reflecting optical waveguides in SiO2-Si multilayer structures," *Appl. Phys. Lett.*, vol. 49, no. 1, pp. 13–15, Jul. 1986.

[36]   P. Yeh, *Optical waves in layered material*. Wiley-Interscience, 2005.

[37]   W. Huang, R.M. Shubair, A. Nathan and L. Chow, "The Modal Characteristics of ARROW Structures," *J. Lighwave Technol.*, vol. 10, no. 8, pp. 1015–1022, 1992.

[38]   M. A. Joffe, W. Ketterle, A. Martin, and D. E. Pritchard, "Transverse cooling and deflection of an atomic beam inside a Zeeman slower," *J. Opt. Soc. Am. B*, vol. 10, no. 12, pp. 2257–2262, Dec. 1993.